Geochemistry Geophysics Geosystems G3

Article
Volume 12, Number 7
13 July 2011
Q07008, doi:10.1029/2011GC003577
ISSN: 1525-2027

Published by AGU and the Geochemical Society

Shear wave modeling and Poisson's ratio in the Variscan Belt of SW Iberia

I. Palomeras
Department of Earth's Structure and Dynamics, Institute of Earth Sciences "Jaume Almera," CSIC, Lluís Solé i Sabarís s/n, E-08028 Barcelona, Spain (ipalomeras@ictja.csic.es)

Now at Department of Earth Science, Rice University, 6100 Main Street, Houston, Texas 77001, USA

R. Carbonell
Department of Earth's Structure and Dynamics, Institute of Earth Sciences "Jaume Almera," CSIC, Lluís Solé i Sabarís s/n, E-08028 Barcelona, Spain (rcarbo@ictja.csic.es)

P. Ayarza
Departamento de Geología, Universidad de Salamanca, Pl. de la Merced s/n, E-37008 Salamanca, Spain (puy@usal.es)

D. Martí and D. Brown
Department of Earth's Structure and Dynamics, Institute of Earth Sciences "Jaume Almera," CSIC, Lluís Solé i Sabarís s/n, E-08028 Barcelona, Spain (dmarti@ictja.csic.es; dbrown@ictja.csic.es)

J. F. Simancas
Departamento de Geodinámica, Universidad de Granada, Av. Fuentenueva s/n, E-19071 Granada, Spain (simancas@ugr.es)

[1] In 2003 two wide-angle reflection/refraction seismic transects were acquired in the Variscan Belt of SW Iberia. The approximately 250 and 300 km long, dense trace spacing transects revealed clear S wave arrivals in the shot gathers recorded by vertical component sensors in both transects. First S wave arrivals (*Sg*) and Moho reflections (*SmS*) are the most prominent phases that can be correlated from shot to shot. *Sg* is observed up to relatively large offsets and constrains the upper and middle crust S wave velocities. The *SmS* is seen from offset 0 (18 s twtt) to 150 km offset, where it intercepts first S wave arrivals (*Sg*). The upper mantle refracted phase (*Sn*) is difficult to recognize, although *PmS/SmP* converted phases can be identified. Using a 2-D ray tracing approach, two S wave velocity models for the crust of SW Iberia were obtained. These S wave velocity models complement the previous P wave velocity models and provide us with relatively well resolved Poisson's ratio crustal sections for SW Iberia. The resulting Poisson's ratio models present differences between tectonic zones at upper and middle crustal depths, thus supporting the existence of different tectonic zones prior to the Variscan collision. The most noteworthy feature is the high Poisson's ratio value (over 0.28) coincident with high P wave velocity areas (over 6.8 km/s) at midcrustal depths. In order to constrain the possible crustal composition, P wave velocities and Poisson's ratios have been compared with published laboratory measurements on different crustal rock types. This comparison indicates that the high P wave velocity and Poisson's ratios are compatible with a mixture of mafic to ultramafic rock types alternating with felsic ones. This result is consistent with the existence of mafic layered bodies in the middle crust, in the same way that has been suggested by previous works in this area.

Components: 11,300 words, 11 figures, 2 tables.

Keywords: Poisson's Ratio; S-wave modeling; SW-Iberia; Variscan Belt; Wide-angle.

Index Terms: 0905 Exploration Geophysics: Continental structures (8109, 8110); 0935 Exploration Geophysics: Seismic methods (3025, 7294); 1020 Geochemistry: Composition of the continental crust.

Received 22 February 2011; **Revised** 18 May 2011; **Accepted** 25 May 2011; **Published** 13 July 2011.

Palomeras, I., R. Carbonell, P. Ayarza, D. Martí, D. Brown, and J. F. Simancas (2011), Shear wave modeling and Poisson's ratio in the Variscan Belt of SW Iberia, *Geochem. Geophys. Geosyst.*, *12*, Q07008, doi:10.1029/2011GC003577.

1. Introduction

[2] Estimates of the continental crustal composition are important to understand the evolution and growth of the continents, but direct sampling to address this issue is unfeasible. Physical properties, like seismic velocities, obtained by indirect techniques (wide-angle reflection/refraction seismic prospection) has proven to be a useful tool for estimating the composition of the crust and even the lithosphere when compared with laboratory measurements [e.g., *Shillington et al.*, 2004; *Palomeras et al.*, 2009]. Nevertheless, laboratory measurements of P and S wave velocities for different rock types [e.g., *Christensen and Mooney*, 1995] show that many of these have similar values, making it difficult to differentiate between them. Poisson's ratios or V_p/V_s, however, may place key constraints on the crustal composition [e.g., *Holbrook*, 1988; *Brown et al.*, 2003; *Hauser et al.*, 2008; *Janik et al.*, 2009]. Because of the relatively small range of values that the Poisson's ratio features for crustal rocks (from 0.22 to 0.35), high resolution on its determination is required.

[3] SW Iberia presents the best exposed fragment of the Variscan orogenic Belt, that was developed under a transpressional tectonic regime. This region provides a good opportunity to study this orogeny and its evolution. In this study we present two S wave velocity models and the resulting Poisson's ratio variations obtained for the crust of the SW Iberian Peninsula. The models have been derived from the IBERSEIS Wide-Angle experiment data set [*Palomeras et al.*, 2009], which is composed of two ~300 km long transects that cross the Variscan Belt of SW Iberia (Figure 1). This project was designed to study the composition of the lithosphere of SW Iberia and complement the previous normal incidence seismic survey IBERSEIS [*Simancas et al.*, 2003; *Carbonell et al.*, 2004; *Schmelzbach et al.*, 2008]. The high-resolution recordings have allowed us to identify with confidence strong P waves and high-quality S waves in the vertical seismic recorders. The new S wave velocity models presented here have been integrated with the P wave models derived from the same transects [*Palomeras et al.*, 2009] and have led to the computation of Poisson's ratio models. The Poisson's ratio models derived for each transect have been compared with published experimental data [*Christensen*, 1996] to obtain petrological information of the crust and to create a lithological model of the area.

2. Geological Setting

[4] The Variscan Belt is a Late Paleozoic orogen that extends along most of Europe. The western half of the Iberian Peninsula represents a continuous outcrop (the Iberian Massif) of the Variscan Belt. In SW Iberia, the Variscan Belt is made up of three continental blocks: the South Portuguese Zone (SPZ), the Ossa-Morena Zone (OMZ) and the Central Iberian Zone (CIZ) (Figure 1). The latter one represents the autochthonous margin of Gondwana [*Pérez-Estaún and Bea*, 2004]. The OMZ crust is also ascribable to the margin of Gondwana, but its boundary with the CIZ is a major tectonic band that suggests some degree of independence for the OMZ [*Azor et al.*, 1994; *Simancas et al.*, 2009]. In turn, the boundary between the OMZ and the SPZ is considered to be the place where the Rheic Ocean closed, giving way to the collision between the Avalonian margin of Laurussia and the margin of Gondwana [*Matte*, 2001].

[5] In between the autochthonous CIZ and the exotic SPZ, the OMZ is a key piece of crust whose stratigraphy records a Paleozoic evolution characterized by a rifting event from Early-Middle Cambrian to Ordovician, a passive margin stage from Ordovician to Early Devonian and a complex synorogenic evolution during Devonian and Carboniferous times [*Simancas et al.*, 2001; *Robardet and Gutíerrez-Marco*, 2004]. The OMZ/CIZ boundary is a wide shear zone dominated by left-lateral displacement,

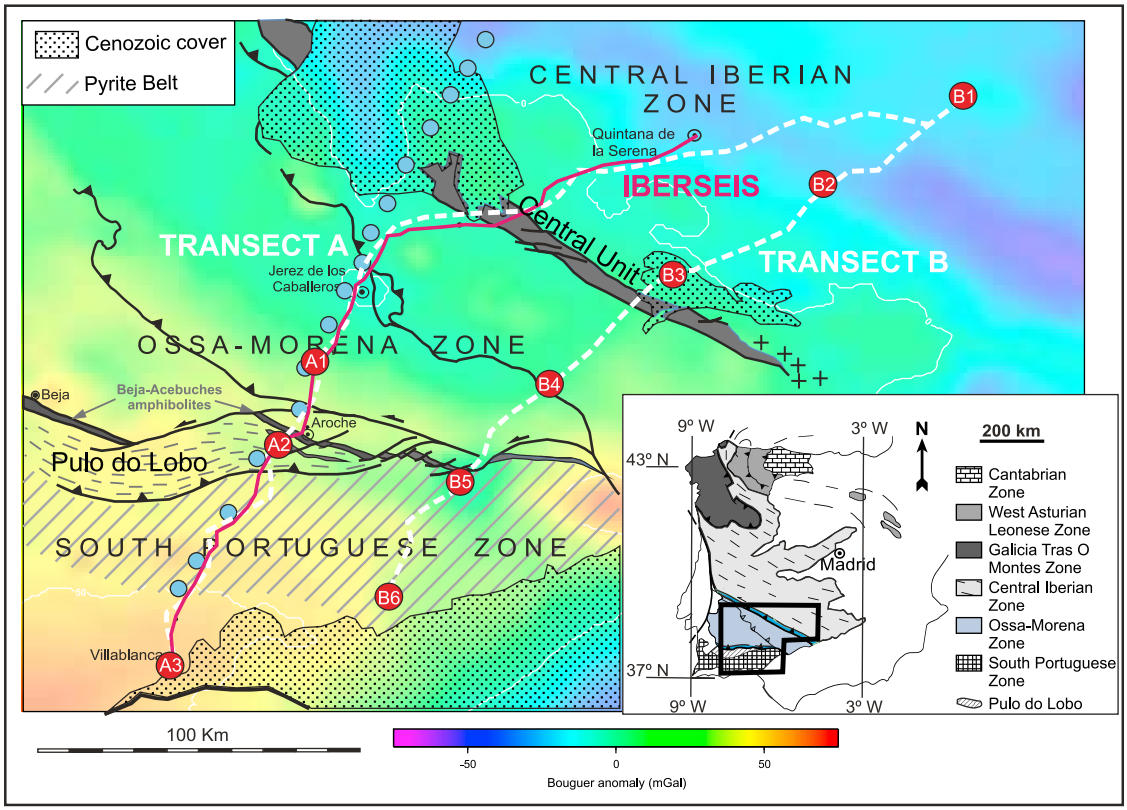

Figure 1. Map of the main geological units and tectonic zones of SW Iberia placed on the top of the Bouguer anomaly map. The location of the two wide-angle seismic reflection profiles, transect A and transect B (white dashed lines), and the shot positions (red circles) are shown. The acquisition parameters are specified in the text and in Table 1. The normal incidence seismic profile IBERSEIS is shown as a red line. Light blue circles indicate the magnetotelluric station locations.

which includes eclogite lenses, mafic rocks of MORB affinity and a variety of high-grade gneisses and metasediments [*Burg et al.*, 1981; *Azor et al.*, 1994; *Ordoñez Casado*, 1998; *Gómez-Pugnaire et al.*, 2003]. Furthermore, a vergence change of the Variscan structures takes place at this boundary [*Simancas et al.*, 2001]. These features, together with some differences in the Paleozoic stratigraphy with respect to the CIZ, have led to suggest that this is a major orogenic Variscan boundary, though faunal affinities between the OMZ and the CIZ do not substantiate a significant separation between them [*Robardet and Gutíerrez-Marco*, 2004].

[6] The SPZ is the southernmost crustal piece in SW Iberia. It is characterized by extensive outcrops of magmatic rocks of Early Carboniferous age, related to the famous giant sulphide deposits in the region [*Sáez et al.*, 1999]. The SPZ outcrops reveal a Middle Devonian to Carboniferous stratigraphy, and cannot be compared with the OMZ and CIZ concerning the Early Paleozoic evolution. However, the SPZ crust is interpreted as exotic with respect to the OMZ and CIZ because its boundary with the OMZ is an orogenic suture, based on the presence of three particular units: the Pulo do Lobo (PL), the Allochthonous Complex of southern OMZ and the Beja-Acebuches amphibolites. The Pulo do Lobo unit, is made up of low-grade schists and quartzites crowded with quartz veins and including oceanic-type metabasalts. It has been interpreted as a subduction-related accretionary prism [*Eden and Andrews*, 1990; *Oliveira*, 1990]. The Allochthonous Complex is dominated by the Moura-Cubito schists and tectonic lenses of oceanic-type metabasites, nonoceanic eclogitic metabasites, gneisses and high-grade marbles and schists. This ensemble may represent an accretionary complex from a continental margin, plus small obducted pieces of oceanic crust [*Fonseca et al.*, 1999; *Araújo et al.*, 2005]. Finally, the Beja-Acebuches amphibolites are a continuous outcrop of metabasic rocks along this boundary (OMZ/SPZ) and have been interpreted as an ophiolite of the Rheic Ocean [*Fonseca and Ribeiro*, 1993; *Quesada et al.*, 1994; *Castro et al.*, 1996], though the Early Carboniferous age recently

determined for these metabasites does not support that interpretation [*Azor et al.*, 2008]. Despite these new geochronological data, the boundary between the OMZ and the SPZ may still be considered an orogenic suture, based mainly on the Pulo do Lobo and the Allochthonous Complex evidence.

[7] Early Carboniferous mafic magmatism is a particular feature of SW Iberia. Together with prominent volcanism in the SPZ, basalts are common in the Early Carboniferous basins of the OMZ and southern CIZ [*Simancas et al.*, 2001]. Moreover, on the basis of reflection seismic data, magmatic rocks have been interpreted to occur in the upper crust of SW Iberia [*Simancas et al.*, 2003; *Carbonell et al.*, 2004; *Schmelzbach et al.*, 2008; *Palomeras et al.*, 2009, 2011]. The tectonic interpretation of this significant magmatic intraorogenic event is open to debate: it might be a hot spot related to some type of mantle plume impinging on SW Iberia and the neighboring Canadian Maritimes [*Simancas et al.*, 2006] or it might be due to orogenic slab breakoff [*Pin and Rodríguez*, 2009].

[8] To sum up, the Paleozoic orogenic evolution of SW Iberia is recorded in the tectonothermal evolution of three continental blocks: SPZ, OMZ, and CIZ, whose collision has produced two orogenic sutures, at the boundaries of the OMZ. One of these boundaries (OMZ/SPZ) may be the scar of the Paleozoic Rheic Ocean. The continental collision started in Devonian times, but a likely hot spot stage, manifested in mafic acid magmatism and extension, took place in SW Iberia during the Early Carboniferous. Further description and discussion on the tectonic evolution of the Variscan orogen in Iberia can be found elsewhere [*Simancas et al.*, 2003; *Pérez-Estaún and Bea*, 2004].

3. Geophysical Background

[9] Several geophysical studies have been carried out in SW Iberia. One of the most important ones is the IBERSEIS vertical incidence experiment, a ~300 km long normal incidence seismic survey acquired in 2001 [*Simancas et al.*, 2003]. This survey crossed the SPZ, the OMZ and the CIZ and their tectonic boundaries (Figure 1) providing a very detailed seismic image of the crust. This image provided new structural data on the Variscan Belt at crustal scale revealing the geometry of the structures. The most remarkable feature imaged by this seismic profile was the Iberseis Reflective Body (IRB) [*Simancas et al.*, 2003; *Carbonell et al.*, 2004], a thick, 175 km long and irregular reflective band located within the OMZ and CIZ at a depth between 4.5 s and 6.0 s two way traveltime (twtt). The image of the IRB shows bands of reflectivity, that has led the authors to interpret it as a layering of sill-like mafic and ultramafic igneous rocks with interlayered septa of metasedimentary rocks [*Simancas et al.*, 2003; *Carbonell et al.*, 2004]. The image of the IBERSEIS profile also shows an almost flat and continuous Moho discontinuity at 10.5 s twtt. No remains of either the lower crust subducted in the suture zones or those of a previous orogenic root are observed.

[10] In September 2003 the IBERSEIS wide-angle survey was carried out in the same area (Figure 1). It consisted of two high-resolution wide-angle reflection/refraction transects [*Palomeras et al.*, 2009; *Flecha et al.*, 2009; *Ayarza et al.*, 2010]. Transect A was approximately 300 km long and overlapped the trace of the normal incidence survey IBERSEIS. This transect revealed that the IRB corresponds to an area of high P wave velocities (6.8–6.9 km/s) situated at 12–15 km depth. Transect B was approximately 250 km long and was located to the ESE of transect A, sharing with it the northern end. Results of transect B show the nonuniqueness of the IRB, revealing the existence of more high-velocity bodies, now within the SPZ and CIZ, also at midcrustal depths. Both transects also show an almost flat Moho discontinuity situated at 32 km depth. *Palomeras et al.* [2009] suggested a possible crustal composition along both transects comparing the wide-angle compressional wave velocities with laboratory measurements corrected for depth and temperature. These authors conclude that the midcrustal high velocities are consistent with the existence of mantle derived rocks.

[11] *Flecha et al.* [2009] studied the reflectivity observed in the IBERSEIS wide-angle shot gathers at middle to lower crustal levels and at the Moho generating synthetic seismograms using a 2-D finite elements elastic approach. In order to reproduce the observed seismic signature (high amplitude and reverberatory coda) the original model (forward model obtained by *Palomeras et al.* [2009]) had to be perturbed by introducing randomly distributed ellipses with velocity variations of ±0.2 km/s within the middle and lower crust. The resulting synthetic seismograms qualitatively reproduce more accurately the shot records than the one generated by the unperturbed model. This study concluded that the high P wave velocity zones could correspond to a layered mafic intrusion and that the lower crust and Moho may be strongly laminated.

Table 1. Data Acquisition Parameters for Transect A and Transect B

Description	Transect A	Transect B
Intershot distance	approximately 60 km	approximately 60 km
Number of shots	6 shots (3 mistaken)	6 shots fired twice
Shot charges (kg)	A1:1000, A2:750, A3:500	B1:1000, B2:750, B3:500 B4:500, B5:750, B6:1000
Charge configuration	single 50–60 m borehole	single 50–60 m borehole
Station spacing	400 m	approximately 150 m
Length of profile	~300 km	~250 km

[12] Additionally, modeling studies using geopotential fields have also been carried out in SW Iberia. *Palomeras et al.* [2011] obtained two lithospheric-scale models of SW Iberia using a code that combines heat flow, gravity, geoid elevation and topography [*Zeyen and Fernàndez*, 1994]. The models run from across the Gulf of Cadiz to the CIZ, crossing the SPZ and the OMZ, and overlapping the IBERSEIS wide-angle transects. Resulting lithospheric models revealed that high-density bodies are needed at midcrustal depths in order to fit the geopotential fields. The positions and shapes of these high-density bodies closely coincide with those of the high P wave velocity bodies. Previous modeling studies using a similar algorithm were carried out in the area [*Fernàndez et al.*, 2004]. These models needed to thicken the middle crust and decrease the thickness of the upper crust within the OMZ in order to increase the crustal density to account for the geopotential fields signature.

[13] Finally, a magnetotelluric profile was also acquired in the study area in 2001 [*Pous et al.*, 2004] largely coincident with the IBERSEIS seismic profile (Figure 1). The resulting resistivity model shows that the IRB coincides with the top of a 120 km long high-conductivity layer located at midcrustal depths [*Carbonell et al.*, 2004] and interpreted as a sill-like intrusion of magmas with assimilated pyritic graphite-rich rocks.

[14] Accordingly, all the studied geophysical data sets indicate that the crust in the area is relatively mafic in composition, mostly at middle and lower crustal levels. The tectonic evolution of SW Iberia in Early Carboniferous times, characterized by mafic magmatism, has been addressed as the scenario in which the mafic lithologies identified in the middle deep crust may have originated.

[15] All these multidisciplinary studies have constrained a detailed crustal model. However, to identify specific lithologies, and to reveal differences between the three tectonic zones, additional information and better resolution on the physical properties is needed. Thus constraints on the S wave structure and Poisson's ratio are required.

4. IBERSEIS Wide Angle: S Wave Data

4.1. Data Acquisition

[16] The IBERSEIS Wide-Angle survey consists of two transects acquired in SW Iberia. Both transects cross the main tectonic units (the SPZ, the OMZ and the CIZ) and are perpendicular to their tectonic contacts. The transects were acquired using 650 vertical seismic geophones connected to REFTEK 125A digital recorders (Texans) of the IRIS-PASSCAL instrument pool. Transect A is ~300 km long with a station spacing of approximately 400 m. Transect B is ~250 km long and a denser station spacing was used (approximately 150 m). To achieve this spacing, shots along this transect were fired twice: first the stations were placed at approximately 300 m spacing and after the shots were fired, the stations were moved 150 m toward the north along the profile. Then all shots were fired again. Six shots were designed for each transect (6 + 6 for transect B), but the northern ones on transect A failed. Shot charges were placed in a single 50–60 m deep borehole. Charges used were 1000, 750 and 500 kg. The largest charges were located at the edges of the transects and charge sizes were decreased for the shots toward the center of the transects. The acquisition parameters are summarized in Table 1. Additionally details on the acquisition and P wave processing and interpretation are given by *Palomeras et al.* [2009].

4.2. Data Processing

[17] In order to increase the signal of the S wave phases, the following processing steps were applied to the shot gathers. First, the geometry information obtained by GPS measurements was introduced in the trace headers. The geometry information was used to sort the traces to generate each shot gather

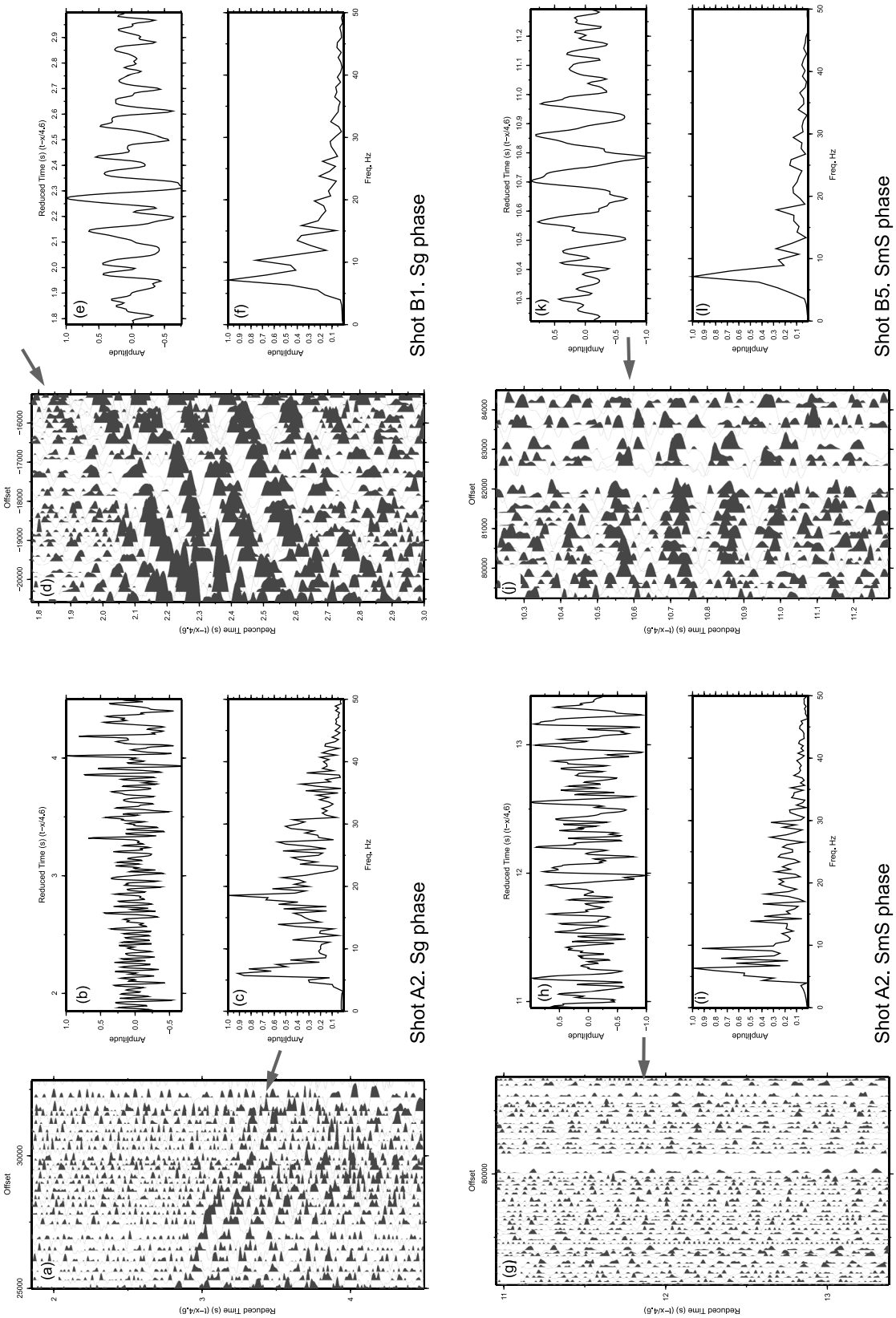

Figure 2. Amplitude spectra of the main S wave phases (*Sg* and *SmS*). (a, d, g, and j) Zoomed regions for which the (c, f, i, and l) amplitude spectra are calculated. (b, e, h, and k) The stacked traces resulting from the window in Figures 2a, 2d, 2g, and 2j. Figures 2a, 2d, 2g, and 2j are imaged with a reduced time corresponding to a velocity of 4.6 km/s.

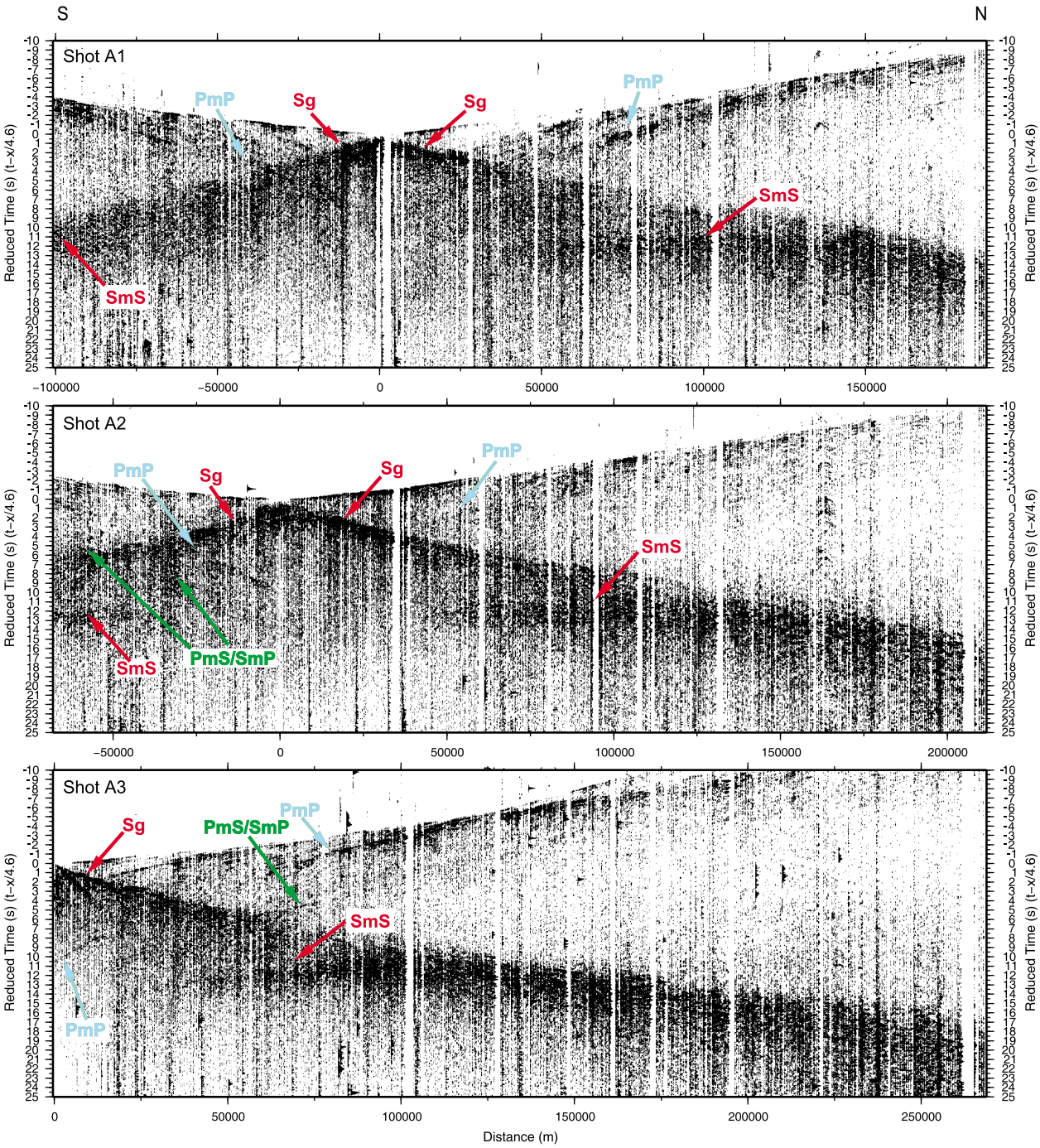

Figure 3. Vertical component record sections for shots acquired along transect A. The data have been band-pass filtered (2–10 Hz). The shot records are displayed with a reduction velocity of 4.6 km/s. The main arrivals which have been interpreted are labeled correspondingly. *Sg* is the first S wave arrival, *SmS* is a S wave reflected from the crust mantle transition (Moho discontinuity), *PmP* is the P wave reflected from the Moho discontinuity, and *PmS*/*SmP* is the P wave incident at the Moho discontinuity and converted in reflection to a S wave or vice versa (converted waves).

before the processing. Then, the traces were balanced, normalizing each trace by an estimate of its background noise. After this, an amplitude balancing (spherical divergence) was applied. This processing step was more important for transect B where each shot record is created by merging two shots. Then, frequency analysis was done (Figure 2). The analysis reveals that the frequency in the most

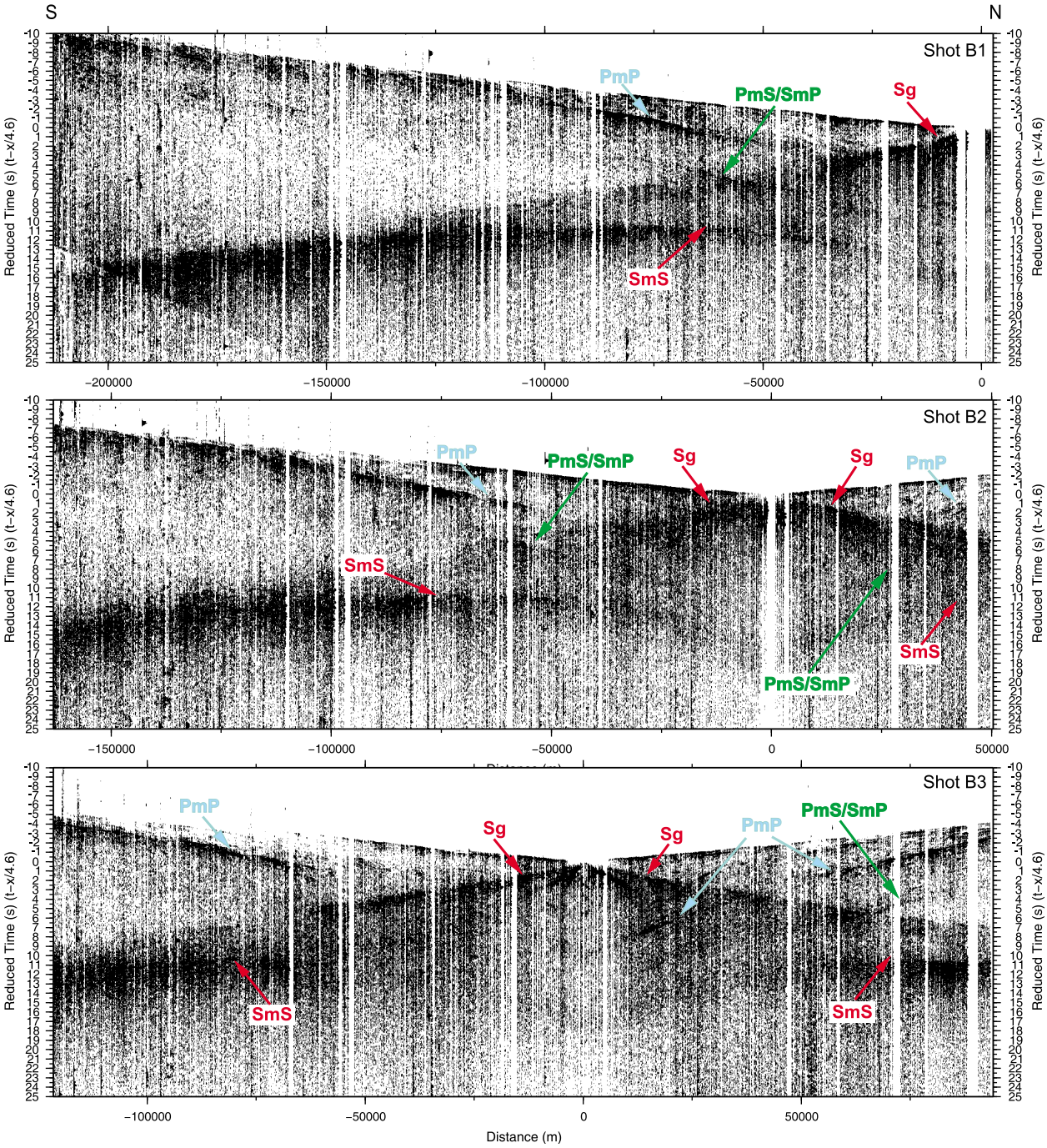

Figure 4. Vertical component record sections for shots acquired along transect B. The data have been band-pass filtered (2–10 Hz). The shot records are displayed with a reduction velocity of 4.6 km/s. The main arrivals which have been interpreted are labeled correspondingly. *Sg* is the first S wave arrival, *SmS* is a S wave reflected from the crust mantle transition (Moho discontinuity), *PmP* is the P wave reflected from the Moho discontinuity, and *PmS*/*SmP* is the P wave incident at the Moho discontinuity and converted in reflection to a S wave or vice versa (converted waves).

prominent S wave phases is lower than 10 Hz. After the frequency analysis, a band pass filter from 2 to 10 Hz (0.25,2,10,15 Hz) was applied to the shot gathers to improve the data quality and to better identify the S wave phases.

4.3. Data Description

[18] Clear S wave arrivals can be identified in the vertical components records, and can be correlated from shot to shot. Different phase arrivals have been

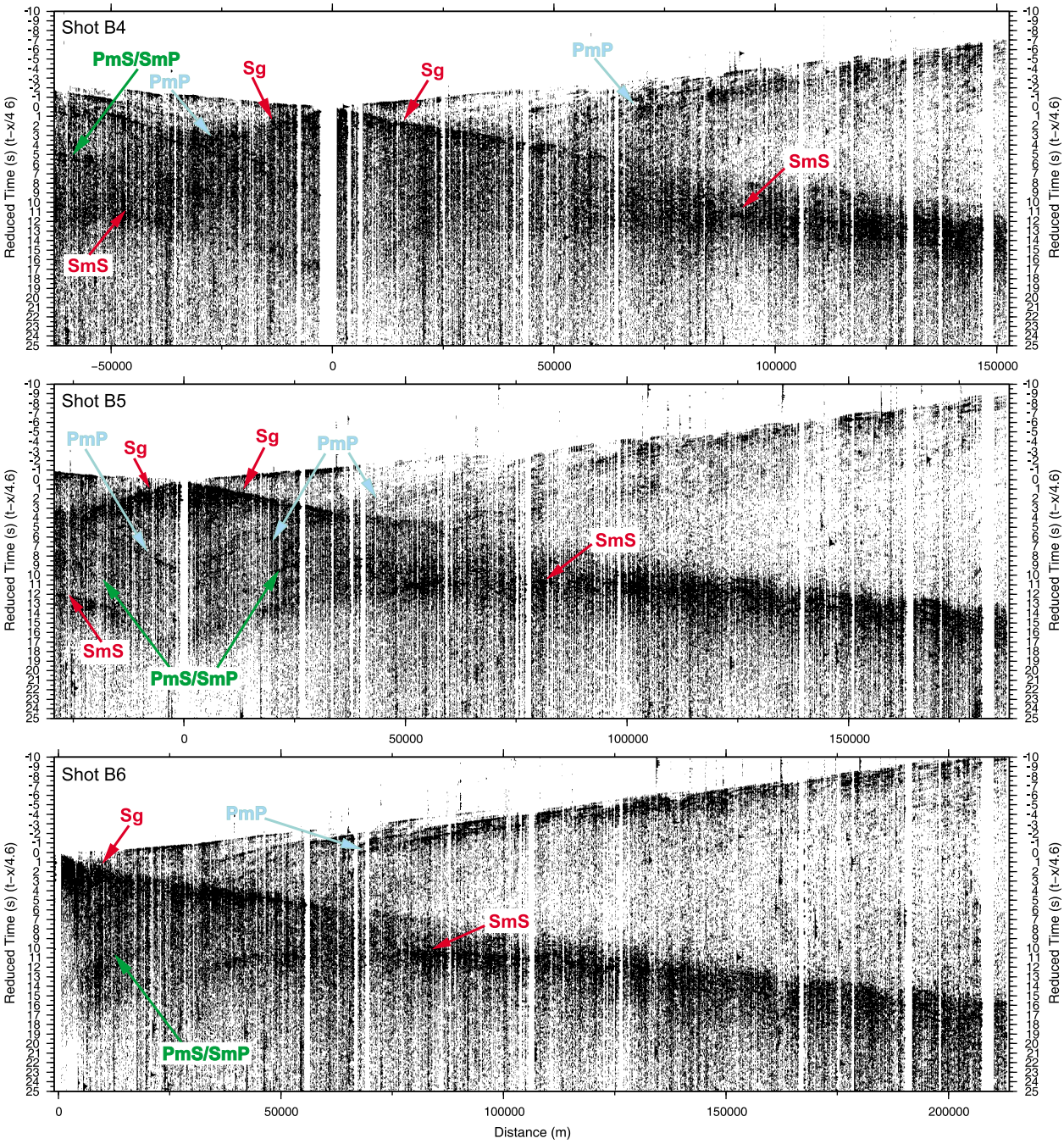

Figure 4. (continued)

identified in the shot gathers (Figures 3 and 4), and they have been labeled following the conventional notation used in refraction experiments. Phases that have been identified, labeled and picked in the shot gathers are (Figures 3 and 4) as follows: (1) *Sg* for the direct arrival of the S waves, (2) *SmS* the reflection of the S waves at the Moho emerging as a S wave, and (3) *PmS/SmP* for the P wave emerging as a S wave or vice versa after reflecting and being converted at the Moho boundary.

[19] The shot gathers present clear intracrustal P wave reflections analyzed and interpreted elsewhere [*Palomeras et al.*, 2009]. However, the intracrustal reflected S wave phases are probably hidden by the P wave energy, making them difficult to recognize. The fact that we are using vertical component

recorders enhances this problem. Accordingly, lesser amplitude S wave phases are expected.

[20] However, the direct first S wave arrival (*Sg*) and the Moho reflection arrival (*SmS*) are very prominent and can be identified and correlated in all record sections. Both, *Sg* and *SmS* phases, have a long coda (up to 2s in some cases). The *Sn* phase (critical refraction at the Moho boundary through the upper mantle) is difficult to recognize because it does not exceed the energy of the compressional waves. In this case, modeling of the subcrustal S wave velocities is not possible. Shot gathers also show converted wave reflections from the Moho (*PmS*/*SmP*). Its presence indicates a sharp crust-mantle transition [*Jacob and Booth*, 1977]. For display purposes all shot gathers are plotted at a reduced time using a $V_s = 4.6$ km/s, that corresponds to $8/\sqrt{3}$ and assumes a Poisson's ratio of 0.25.

4.3.1. Transect A

[21] Shots A1, A2 and A3 show prominent *Sg* arrivals (Figure 3) that appear as a burst of energy with a duration of ~1.5 s. The *Sg* phase can be followed to large offsets, and its changes in slope reveals the presence of as many as 4 layers. The *SmS* phase is observed in all shot gathers from normal incidence until ~150 km offset where it intercepts the *Sg* arrivals. From ~40 km to 150 km offsets it appears as a burst of energy with a ~2 s long coda, while at nearer offsets it appears with a shorter coda and it intercepts the 0 offset at ~18 s twtt. On shot gathers A2 and A3 a converted reflected wave at the Moho (*PmS*/*SmP*) can be observed until offset 0, where it arrives at ~14 s twtt.

4.3.2. Transect B

[22] The six shot gathers along transect B have a relatively high amplitude *Sg* phase (Figure 4). This phase is observed up to large offsets and reveals the presence of, most probably, 5 layers. The Moho reflection (*SmS*) is the most prominent feature in the shot gathers. It can be followed until normal incidence where it also arrives at ~18 s twtt. This phase is characterized by a burst of energy with a 1.5–2 s long coda. As in the shot gathers of transect A, the *PmS*/*SmP* phase is also recognized. This phase intercepts the zero offset at 14 s twtt.

5. Modeling

[23] The S wave velocity models have been obtained by forward modeling using the *Zelt and Smith* [1992] ray tracing based utilities. To use this 2-D ray tracing approach, first the stations and sources of each profile have been projected perpendicularly onto a reference line preserving the offset information.

[24] Although the IBERSEIS wide angle reflection/refraction data set features clear intracrustal P wave reflected phases, no intracrustal S waves reflected phases have been identified. Accordingly, the modeling strategy has been to transform the P wave velocity model from *Palomeras et al.* [2009] into a S wave velocity model using the $V_p/V_s = 1.73$ relationship (assuming a Poisson's ratio of 0.25). Thus, the crustal structure obtained from the P wave modeling has been adopted as a starting S wave model. Next, the upper and middle crustal velocities have been adjusted taking into account the *Sg* phase. The offsets for which the *Sg* is observed are large enough to allow us to model the velocities of the upper ~18 km depth. Finally, the lower crust velocities have been adjusted using the *SmS* arrivals. The Moho depth has been established so that it would be consistent with that of the P wave velocity models [*Palomeras et al.*, 2009] and with the vertical incidence IBERSEIS data [*Simancas et al.*, 2003]. As no *Sn* phase can be identified in the shot gathers, no information about the S wave velocities beneath the Moho can be obtained. Thus, the models presented in this study deal only with the crust.

6. Results: Shear Wave Velocity and Poisson's Ratio Models

[25] As a result of the forward modeling carried out using the criteria described above, a 2-D S wave velocity model has been obtained for each transect (Figures 5b and 6b). It is worth mentioning that the P wave velocity models presented by *Palomeras et al.* [2009], and used as starting models in this work, show high-velocity zones at midcrustal depths. However, these zones cannot be identified in this work.

[26] Variations in the Poisson's ratio in the crust of SW Iberia have been computed from the P wave velocity models of *Palomeras et al.* [2009] and the S wave velocity models presented in this work (Figures 5c and 6c). Poisson's Ratio (σ) as a function of V_p and V_s for an isotropic medium is defined as:

$$\sigma = \frac{1}{2}\left[1 - \frac{1}{(V_p/V_s)^2 - 1}\right] \quad (1)$$

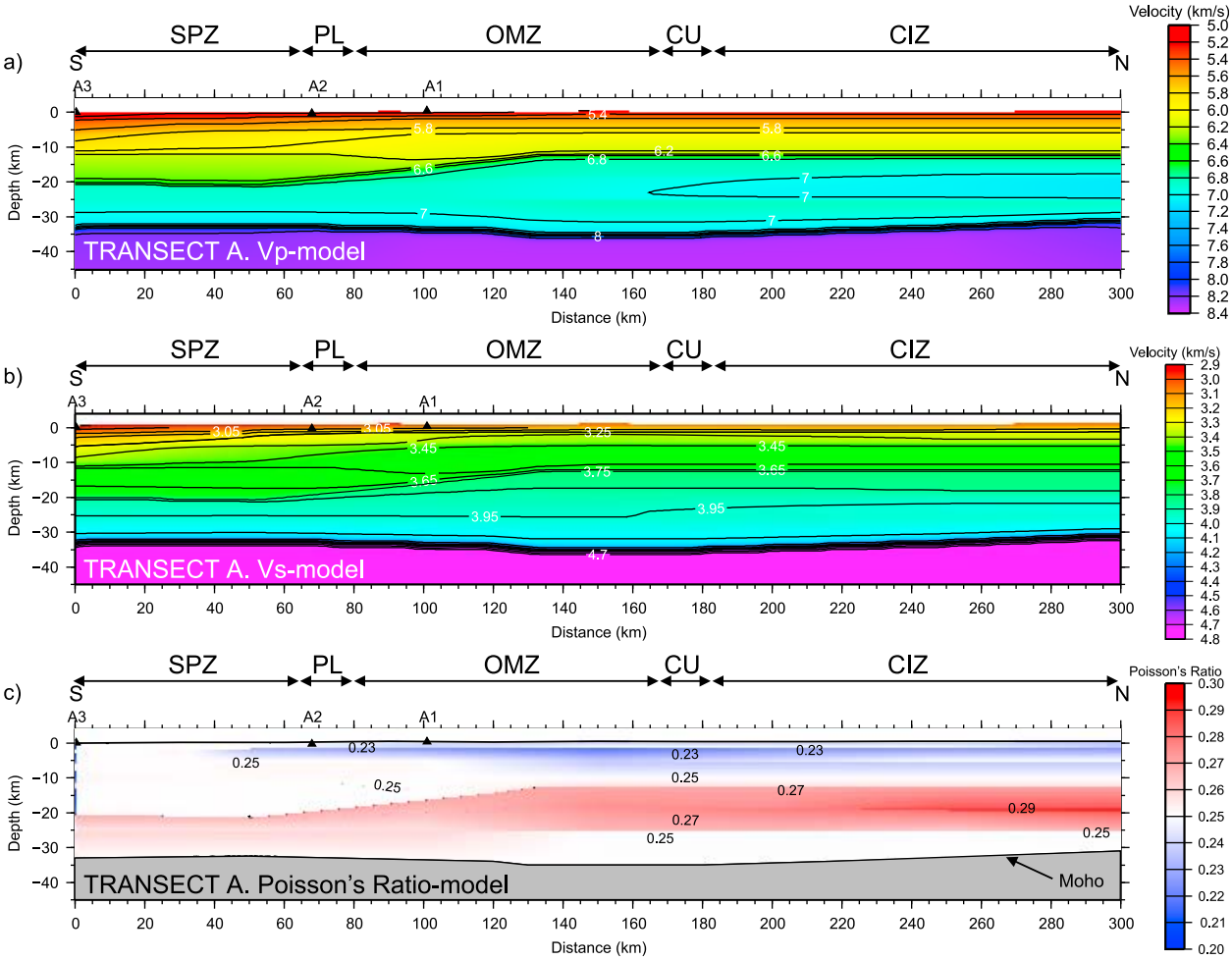

Figure 5. (a) Crustal P wave velocity model for transect A [after *Palomeras et al.*, 2009]. (b) S wave velocity model obtained by iterative ray tracing. (c) Poisson's ratio computed with the P and S wave velocity models. Horizontal arrows represent the tectonic zones in the area (SPZ, South Portuguese Zone; OMZ, Ossa-Morena Zone; CIZ, Central Iberian Zone) and their sutures (PL, Pulo do Lobo; CU, Central Unit). Shot positions are represented as black triangles.

Resulting S wave velocity and Poisson's ratio models for each transect are discussed below.

6.1. Transect A

[27] The S wave velocity model for transect A (Figure 5b) shows some lateral differences along the profile. The upper crust, from 0 to 10–12 km depth, can be divided into two parts: (1) the SPZ and (2) the OMZ and the CIZ. Within the SPZ, the S wave velocities range from 2.90 km/s to 3.45 km/s and are lower than within the northern part where velocities range from 3.10 km/s to 3.60 km/s.

[28] The middle crust extends from 12 km depth down to 20–22 km depth. As in the upper crust, the middle crust also presents lateral differences. Within the SPZ, modeled S wave velocities range from 3.55 km/s to 3.85 km/s, whereas within the OMZ and the CIZ S wave velocities range from 3.75 km/s to 3.95 km/s. The location of the IRB, the high P wave velocity body [*Palomeras et al.*, 2009], corresponds to the mapped area within the OMZ and the CIZ with higher S wave velocities than within the SPZ. The lower crust, from 20–22 km depth to the Moho, is more homogeneous along the transect. At these depths, S wave velocities are similar along the whole transect, ranging from 3.90 km/s to 4.15 km/s.

[29] Poisson's ratios determined for transect A (Figure 5c) show clear differences between the upper, middle and lower crust, and between the various tectonic provinces. The upper crust, from 0 to 12 km depth, shows lower Poisson's ratio values within the OMZ and CIZ than within the SPZ.

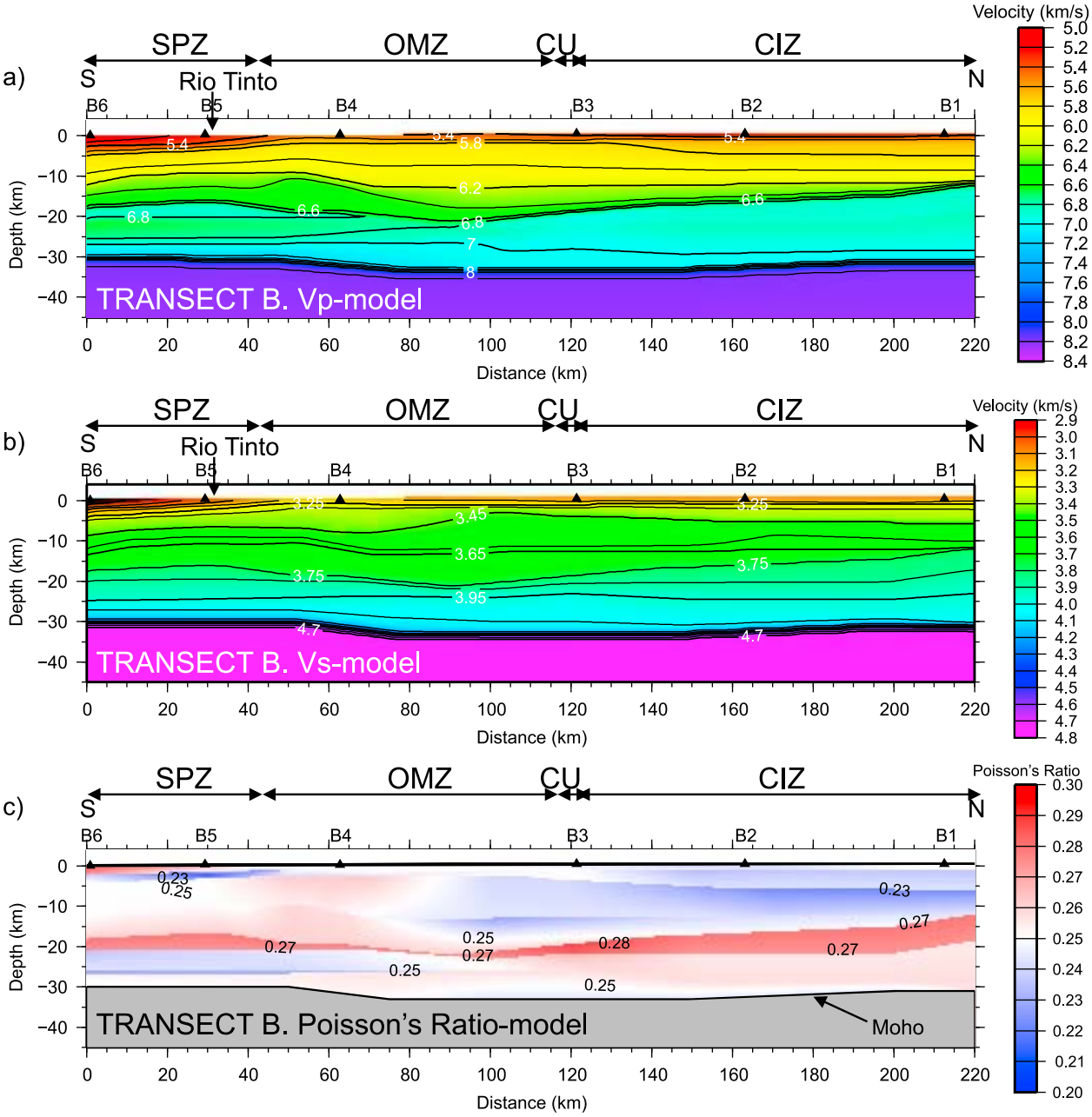

Figure 6. (a) Crustal P wave velocity model for transect B [after *Palomeras et al.*, 2009]. (b) S wave velocity model obtained by iterative ray tracing. (c) Poisson's ratio computed with the P and S wave velocity models. Horizontal arrows represent the tectonic zones in the area (SPZ, South Portuguese Zone; OMZ, Ossa-Morena Zone; CIZ, Central Iberian Zone) and their sutures (PL, Pulo do Lobo; CU, Central Unit). Shot positions are represented as black triangles.

Within the SPZ, Poisson's ratio is 0.25, whereas within the OMZ and CIZ it decreases to 0.23. At midcrustal depths (from 12 to 22 km) the lower Poisson's ratio values are within the SPZ, with values of 0.25. However, Poisson's ratio increases toward the north, within the OMZ and CIZ, up to values of 0.29, coinciding with the high V_p region. The lower crust, from 22 km depth down to the Moho, is more homogeneous, with Poisson's ratio values of 0.25 within the OMZ and CIZ, and slightly higher within the SPZ.

6.2. Transect B

[30] The resulting S wave velocity model for transect B (Figure 6b) is similar to that of transect A. The

S wave velocities in the upper crust (from 0 km to 10–12 km depth) are higher within the OMZ and the CIZ than within the SPZ. Within the SPZ, velocities range from 2.90 km/s to 3.55 km/s, whereas within the OMZ and the CIZ they range from 3.10 km/s to 3.55 km/s. It is noteworthy that the high velocities found beneath shot B4 (km 50 to km 80) at shallow depths (first 2–3 km) are 0.6 km/s higher than the velocities for the rest of the OMZ and CIZ at similar depths.

[31] S wave velocities modeled at midcrustal levels (from 10 km depth to 20 km depth) range from 3.65 km/s to 3.85 km/s. However, the velocity distribution is not homogeneous along the whole transect. In the regions where high P wave velocities are present (SPZ and CIZ), the S wave velocities are higher than within the OMZ for the same depths. In the lower crust (from 20 km depth down to the Moho), S wave velocities range from 3.90 km/s to 4.15 km/s, the same as in transect A.

[32] Poisson's ratio for transect B (Figure 6c) also reveals differences between upper, middle and lower crust, and between tectonic provinces. The upper crust in the northern part of the transect presents lower Poisson's ratio values (0.23). Poisson's ratio increases between 50 and 80 km, underneath shot B4, as do V_p and V_s. Poisson's ratio is relatively high at midcrustal levels (from 10 to 20 km depth). It is higher than 0.27 within the SPZ and than 0.28 within the CIZ coincident with the high P wave velocity areas. Within the OMZ, Poisson's ratio is lower, with values around 0.26. At lower crustal depths, from 20 km down to the Moho, Poisson's ratio increases toward the north, from 0.24 within the SPZ to values greater than 0.25 within the CIZ.

6.3. Model Resolution and Uncertainties

[33] The larger uncertainty in the derived S wave velocity models is for transect A. The fact that the 3 northernmost shots failed reduced the ray coverage in the shallow part and northern part (Figure 7), thus leading to a lack of rays in the velocity model. Consequently, the velocity model is only well controlled in the southern part of the transect for these depths. For transect B, the ray coverage shows that the velocity model is well resolved (Figure 8).

[34] In the analysis of the S wave arrivals, the largest source of error comes from the travel time picking. The S waves have been identified on shot records acquired from vertical component sensors. We have estimated the uncertainty by iterative travel time modeling of domochrones. We have considered a misfit between the observed and modeled arrivals of 0.3–0.5 s (Figures 9 and 10). In the worst case (0.5 s) this results in an error in V_s of ±0.10 km/s.

[35] The Poisson's ratio is directly related to the mineral composition of the rocks. Nevertheless, it is also recognized that crack porosity has a great influence on Poisson's ratio as well as anisotropy. For crystalline rocks, no significant changes in Poisson's ratio have been documented with increasing pressure for pressures above 200 MPa [*Christensen*, 1996; *Wang and Shaocheng*, 2009], when the crack porosity closes.

[36] Although Poisson's ratio helps to place further constraints on possible rock types that make up the crust, we have to consider the uncertainty associated with the calculated V_p and V_s. The standard error in the calculation of the Poisson's ratio could be greater than the variation of the function itself, exceeding the possible coefficient's values [*Hawman et al.*, 1990]. For a V_p/V_s equal to 1.78 and an error in V_p and V_s of 2% we produce an error in the calculated Poisson's ratio of 9% [*Christensen*, 1996]. The error in the Poisson's ratio depends strongly on the V_p/V_s ratio, and it is higher at lower values of V_p/V_s [*Christensen*, 1996]. This uncertainty in the Poisson's ratio is an important consideration when it is calculated from experimental, field and laboratory measurements. For our P and S wave velocity models, the estimated error is 0.15 km/s and 0.10 km/s, respectively. This error produces a Poisson's ratio error of 0.025.

7. Crustal Composition

[37] *Palomeras et al.* [2009] proposed possible lithologies for the crust of SW Iberia from the P wave velocity model. However, this correlation was limited due to the fact that only P wave velocities were used, and similar compressional wave velocities are found for many common crustal rock types [e.g., *Carmichael*, 1989; *Christensen and Mooney*, 1995]. Poisson's ratios determined from P and S wave velocities have the potential of decreasing the range of possible lithologies. In this section we propose possible lithologies for the crust of SW Iberia by comparing the Poisson's ratio models derived from the calculated seismic velocities with the Poisson's ratio measures determined from laboratory measurements. In the absence of laboratory studies on rocks and xenoliths of the area, we used the laboratory measurements made by *Christensen and Mooney* [1995] and *Christensen* [1996] for the most common crustal rock types.

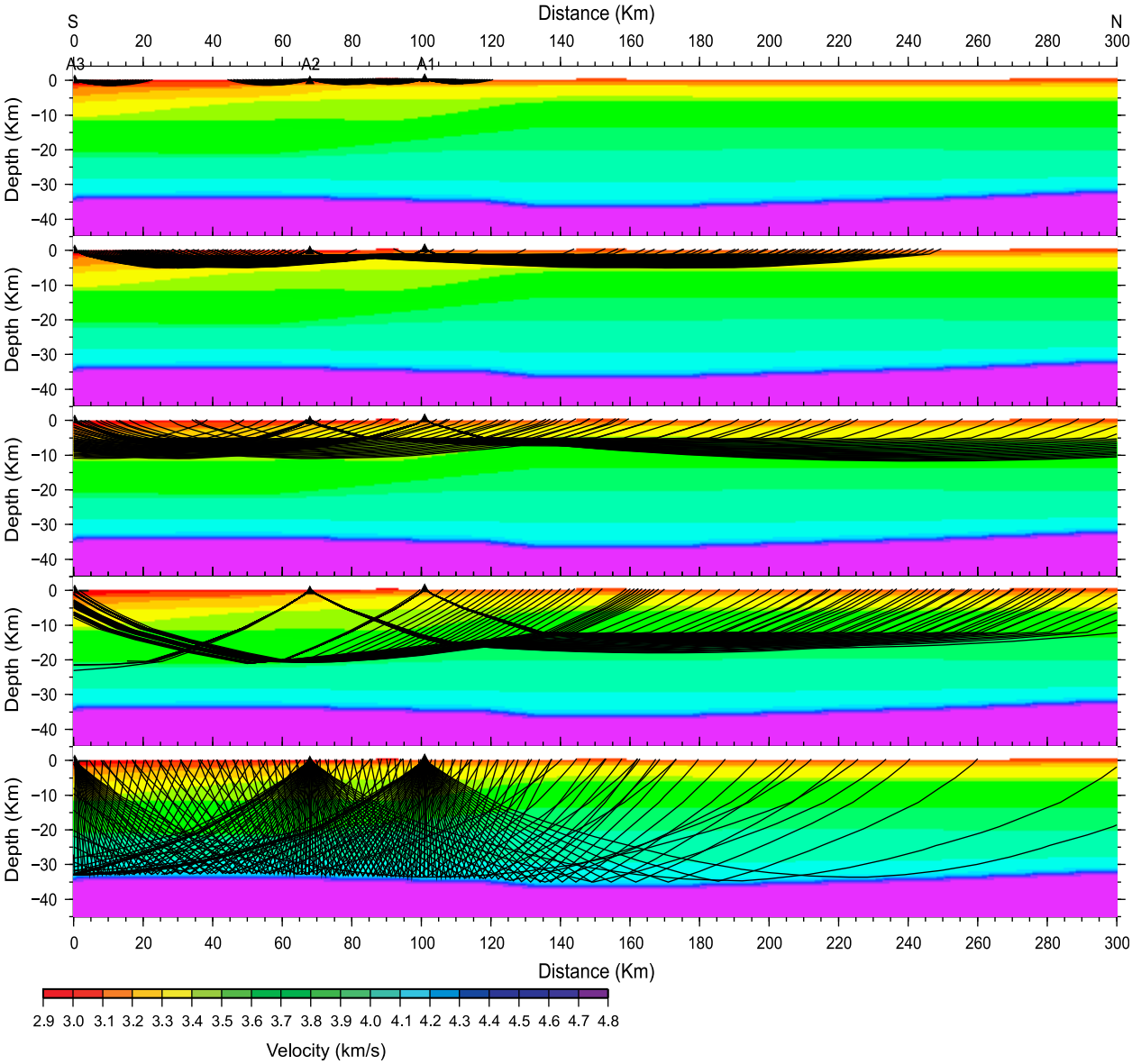

Figure 7. Raypath coverage along transect A for the direct and head waves for crustal discontinuities and for the reflected wave at the Moho (fifth panel). The ray coverage shows the lack of rays in the upper crust for the northern part of the transect.

[38] Changes in pressure and temperature have an influence on the velocity values, and therefore, they have to be taken into account when establishing constraints on crustal composition. However, their influence is low on the Poisson's ratio estimates, and it fluctuates within the experimental error bars [*Christensen*, 1996].

[39] Laboratory derived P wave velocities used in this work have been corrected for depth and temperature with the SW Iberia geotherm (20°C/km) [*Palomeras et al.*, 2011] (Table 2). A qualitatively smoothing procedure has been applied so that areas with similar velocities and Poisson's ratio have been merged into the same structure (layer). Then vertical profiles, V_p/depth and Poisson's ratio/dept have been determined by averaging the values from a 20 km wide strip within each tectonic province and for each profile. The resulting values have been compared with the ones in Table 2 to obtain the possible crustal composition for SW Iberia (Figure 11). Crack porosity has a strong influence on the seismic velocities, especially on the S wave velocities. This produces large deviations in the Poisson's ratios. In most rocks, crack porosity does not close until pressures greater than 100–200 MPa, that corre-

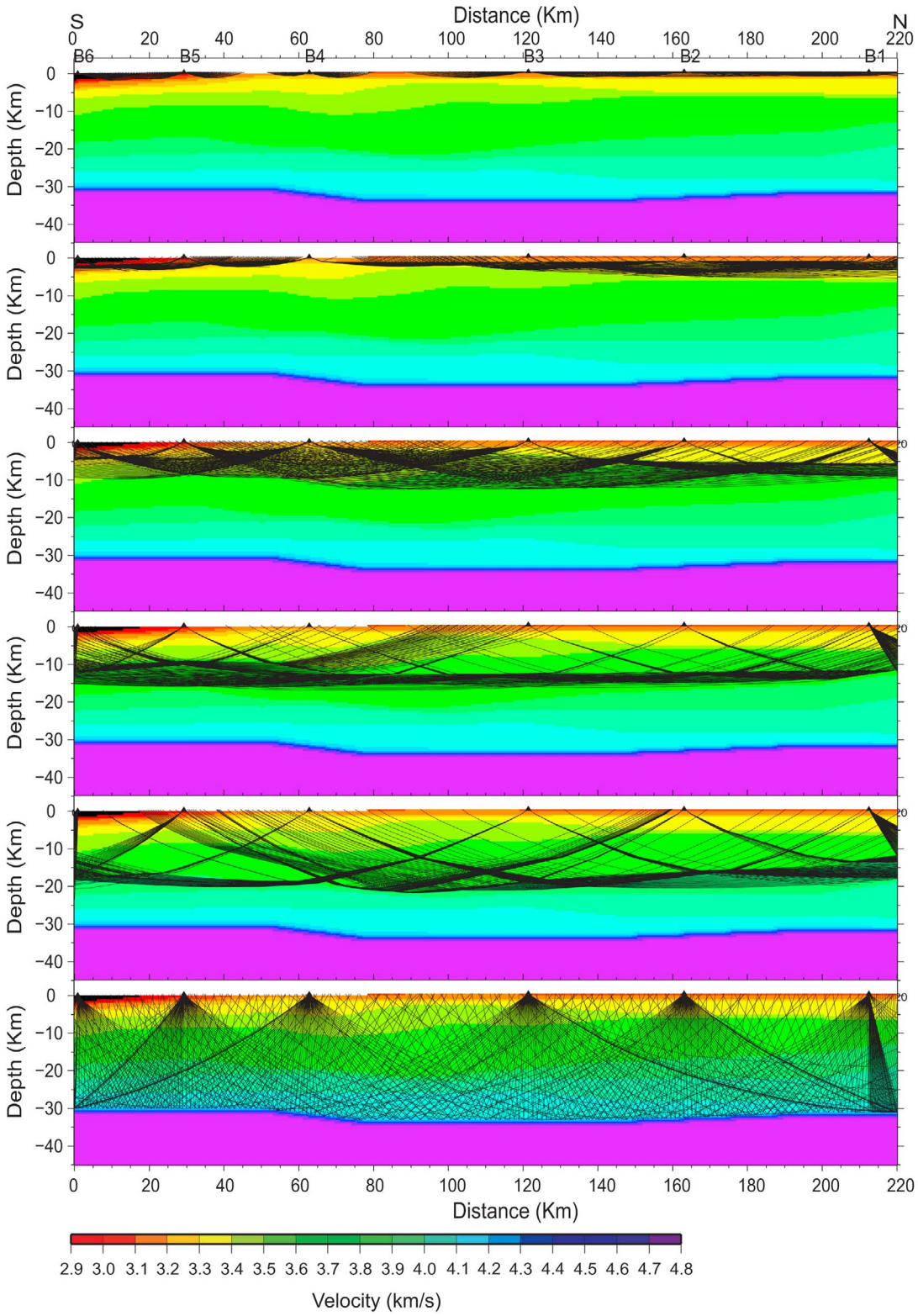

Figure 8. Raypath coverage along transect B for the direct and head waves for crustal discontinuities and for the reflected wave at the Moho (sixth panel). The ray coverage shows that the rays sample the whole transect.

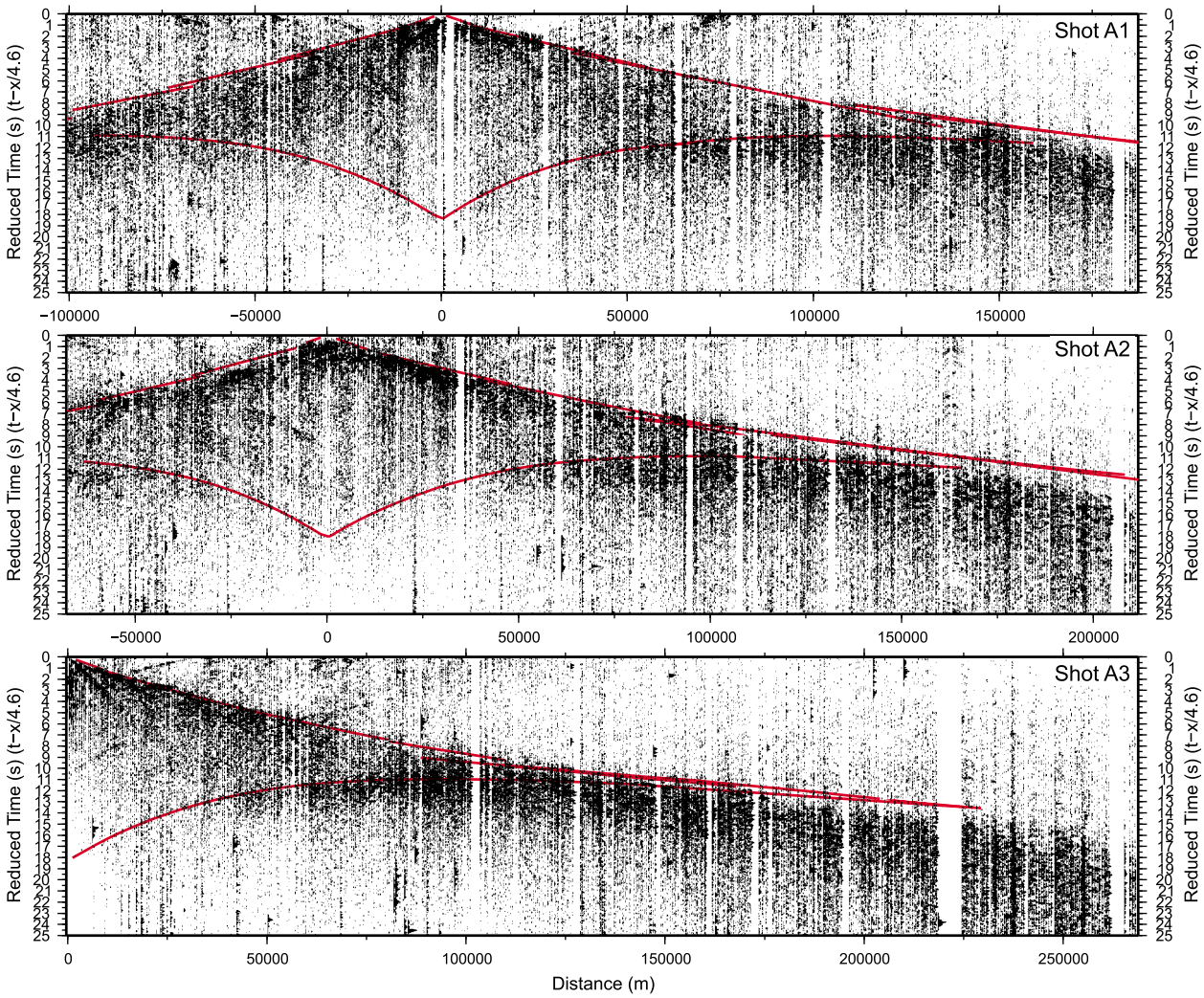

Figure 9. Theoretical traveltime branches predicted by the S wave velocity model of transect A using the *Zelt and Smith* [1992] algorithm. The theoretical traveltime branches illustrate the agreement between the observed phases and the model prediction. The data have the same processing as in Figure 3.

sponds to depths of somewhat less than 10 km (6–7 km depth). Accordingly, the influence of the crack porosity in our models is expected to affect only the uppermost crust.

7.1. Upper Crust

[40] The upper crust can be divided into two layers. The more superficial one (first 2 km) has P wave velocities around 5.1 km/s and Poisson's ratio of 0.25 within the SPZ. Within the OMZ and the CIZ this layer features higher P wave velocity, 5.3 km/s, and lower Poisson's ratio, 0.24. These values are consistent with metagraywacke, a rock type which is dominant in the outcrops of the region. Below, in the southern part of the transects (SPZ), a P wave velocity of 5.9 km/s and Poisson's ratio of 0.25 is obtained, while 6.0 km/s and 0.23 to the north (OMZ and CIZ) is obtained. The most compatible rocks for this region include granite gneiss, though the surface geology suggests a more complex mixture of lithologies, including schist, metasandstones, metavolcanics and metagranitoid intrusions.

7.2. Middle Crust

[41] The P wave seismic velocities in the middle crust are laterally variable for both transects (Figures 5a and 6a). However, resulting models for the S wave seismic velocity show a more homogeneous crust with small lateral changes (Figures 5b and 6b). The resulting Poisson's ratio, is laterally variable at these depths (Figures 5c and 6c), showing values that are relatively high. A Comparison of the

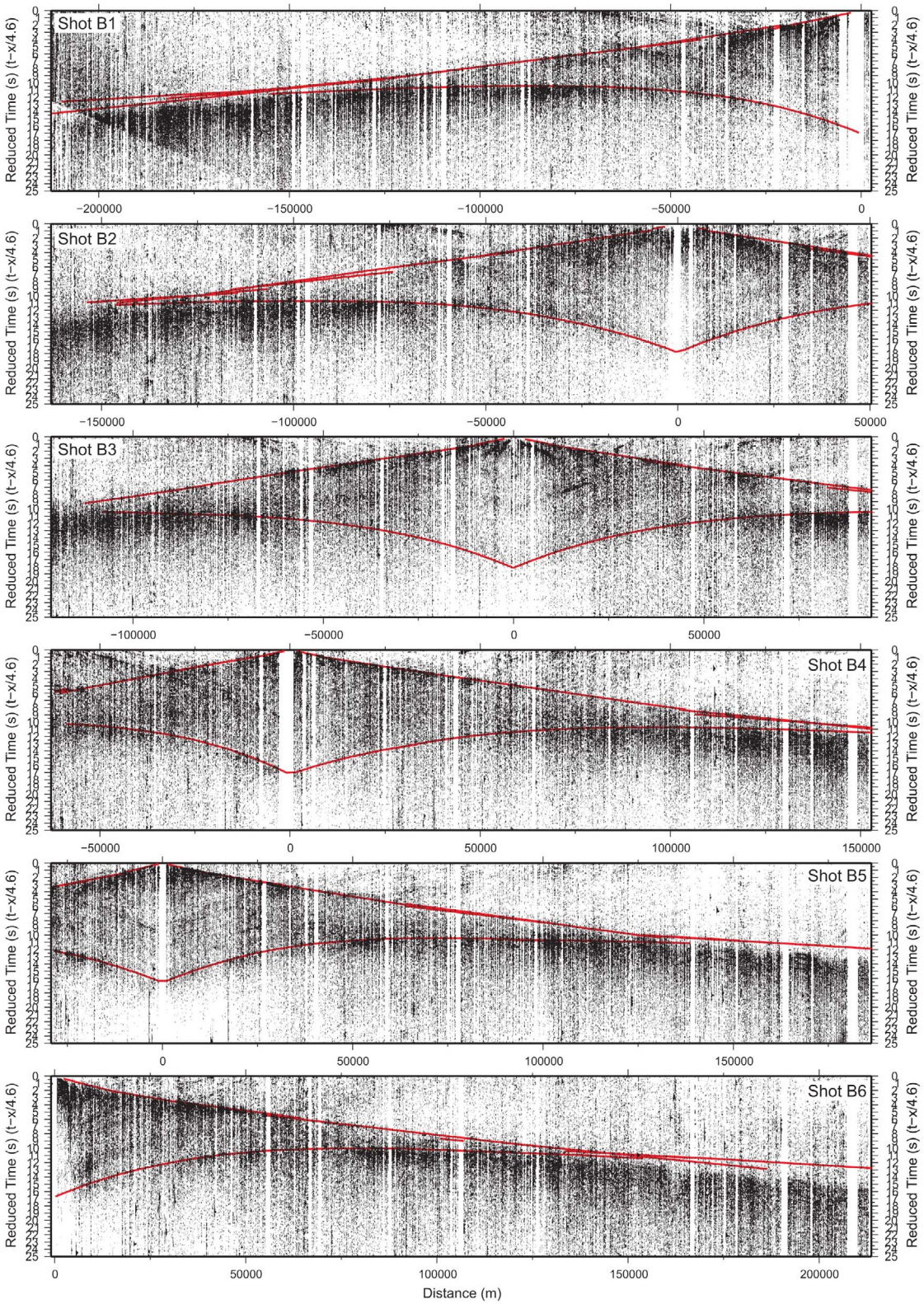

Figure 10. Theoretical traveltime branches predicted by the S wave velocity model of transect A using the *Zelt and Smith* [1992] algorithm. The theoretical traveltime branches illustrate the agreement between the observed phases and the model prediction. The data have the same processing as in Figure 4.

Table 2. Compressional Velocities and Poisson's Ratio (σ) for Different Crustal Rock Types as Functions of Depth and Corrected for Temperature With the SW Iberia Geotherm (20°) [*Palomeras et al.*, 2011][a]

	5 km, 100°C		10 km, 200°C		15 km, 300°C		20 km, 400°C		25 km, 500°C		30 km, 600°C	
	V_p	σ	V_p	σ	V_p	σ	V_p	σ	V_p	σ	V_p	σ
Basalt (BAS)	5.84	0.289	5.87	0.290	5.88	0.291	5.88	0.293	5.87	0.294	5.86	0.295
Diabase (DIA)	6.63	0.277	6.64	0.277	6.63	0.278	6.61	0.278	6.58	0.279	6.56	0.279
Granite-Granodiorite (GRA)	6.17	0.236	6.20	0.237	6.20	0.238	6.18	0.239	6.16	0.239	6.13	0.240
Diorite (DIO)	6.40	0.260	6.45	0.261	6.46	0.263	6.45	0.265	6.43	0.266	6.42	0.268
Gabbro-Norite (GAB)	7.04	0.292	7.05	0.293	7.03	0.294	7.01	0.295	6.98	0.295	6.94	0.296
Metagraywacke (MGW)	5.33	0.238	5.44	0.242	5.51	0.245	5.54	0.248	5.57	0.252	5.58	0.255
Slate (SLT)	6.06	0.298	6.09	0.298	6.11	0.297	6.11	0.297	6.11	0.297	6.09	0.297
Phyllite (PHY)	6.07	0.261	6.13	0.262	6.14	0.263	6.13	0.264	6.12	0.265	6.10	0.266
Zeolite facies Basalt (BZE)	6.24	0.293	6.29	0.294	6.31	0.295	6.31	0.297	6.30	0.298	6.28	0.299
Prehnite-pumpellyite Facies basalt (BPP)	6.24	0.273	6.30	0.274	6.32	0.276	6.32	0.278	6.31	0.279	6.30	0.281
Greenschist facies Basalt (BGR)	6.64	0.260	6.73	0.260	6.75	0.261	6.74	0.262	6.73	0.263	6.71	0.264
Granite gneiss (GGN)	5.99	0.243	6.08	0.245	6.09	0.246	6.09	0.248	6.08	0.250	6.07	0.251
Biotite (tonalite) Gneiss (BGN)	6.09	0.252	6.16	0.253	6.17	0.254	6.17	0.256	6.15	0.257	6.13	0.258
Mica quartz Schist (QSC)	6.16	0.267	6.26	0.268	6.30	0.269	6.30	0.270	6.29	0.270	6.29	0.271
Amphibolite (AMP)	6.74	0.259	6.81	0.260	6.81	0.261	6.79	0.262	6.76	0.263	6.73	0.264
Felsic granulite (FGR)	6.30	0.267	6.33	0.268	6.32	0.269	6.30	0.271	6.27	0.272	6.23	0.273
Paragranulite (PGR)	6.23	0.263	6.27	0.264	6.26	0.265	6.24	0.266	6.21	0.266	6.17	0.267
Anorthositic Granulite (AGR)	6.78	0.295	6.81	0.295	6.80	0.296	6.77	0.297	6.74	0.298	6.71	0.299
Mafic granulite (MGR)	6.74	0.282	6.77	0.282	6.76	0.283	6.73	0.283	6.70	0.283	6.67	0.283
Mafic garnet Granulite (GGR)	6.97	0.272	7.05	0.273	7.05	0.274	7.04	0.276	7.02	0.277	6.98	0.278
Serpentinite (SER)	5.24	0.342	5.26	0.345	5.25	0.347	5.24	0.350	5.21	0.353	5.18	0.355
Quartzite (QTZ)	5.88	0.072	5.90	0.077	5.88	0.083	5.85	0.088	5.81	0.093	5.77	0.099
Calcite marble (MBL)	6.80	0.310	6.81	0.306	6.79	0.303	6.76	0.300	6.73	0.296	6.69	0.293
Anorthosite (ANO)	6.85	0.311	6.88	0.311	6.88	0.312	6.86	0.312	6.84	0.312	6.81	0.313
Hornblendite (HBL)	7.05	0.256	7.08	0.256	7.06	0.257	7.03	0.258	7.00	0.259	6.96	0.260
Pyroxenite (PYX)	7.66	0.253	7.67	0.254	7.66	0.255	7.64	0.257	7.61	0.258	7.57	0.259

[a]Modified from *Christensen and Mooney* [1995] and *Christensen* [1996].

resulting V_p-Poisson's ratio pairs with those of typical rock lithologies measured in the laboratory at high confining pressures and temperatures, shows the following differences between transects and tectonic provinces.

[42] For transect A, the P wave velocities at these depths, increase dramatically toward the north. Within the SPZ the average velocity is 6.3 km/s and average Poisson's ratio is 0.25. Rock types compatible with these measurements include: granite-granodiorite, biotite (tonalite) gneiss, phyllite, paragranulite, mica quartz schist, felsic granulite, diorite and gabbro.

[43] Within the OMZ P wave velocity and Poisson's ratio increase up to 6.9 km/s and 0.26 respectively. The compatible rocks include: greenschist facies basalt, amphibolites, mafic granulite, mafic garnet granulite and hornblendite. Within the CIZ, P wave velocity is 7.0 km/s and Poisson's ratio is around 0.28. Hornblendite, amphibolite, mafic garnet granulite and gabbro-norite-troctolite are rock types compatible at this depth with these values.

[44] For transect B at midcrustal depth, the V_p and Poisson's ratio indicate differences between tectonic provinces but at the same time, there are some similarities. The SPZ and CIZ have two layers with different V_p and Poisson's ratio. The upper part of the middle crust within the SPZ and the middle crust within the OMZ have the same P wave velocity (6.4 km/s) and Poisson's ratio (0.25). The compatible lithologies include: paragranulite, mica quartz schist, felsic granulite, prehnite-pumpellyte facies

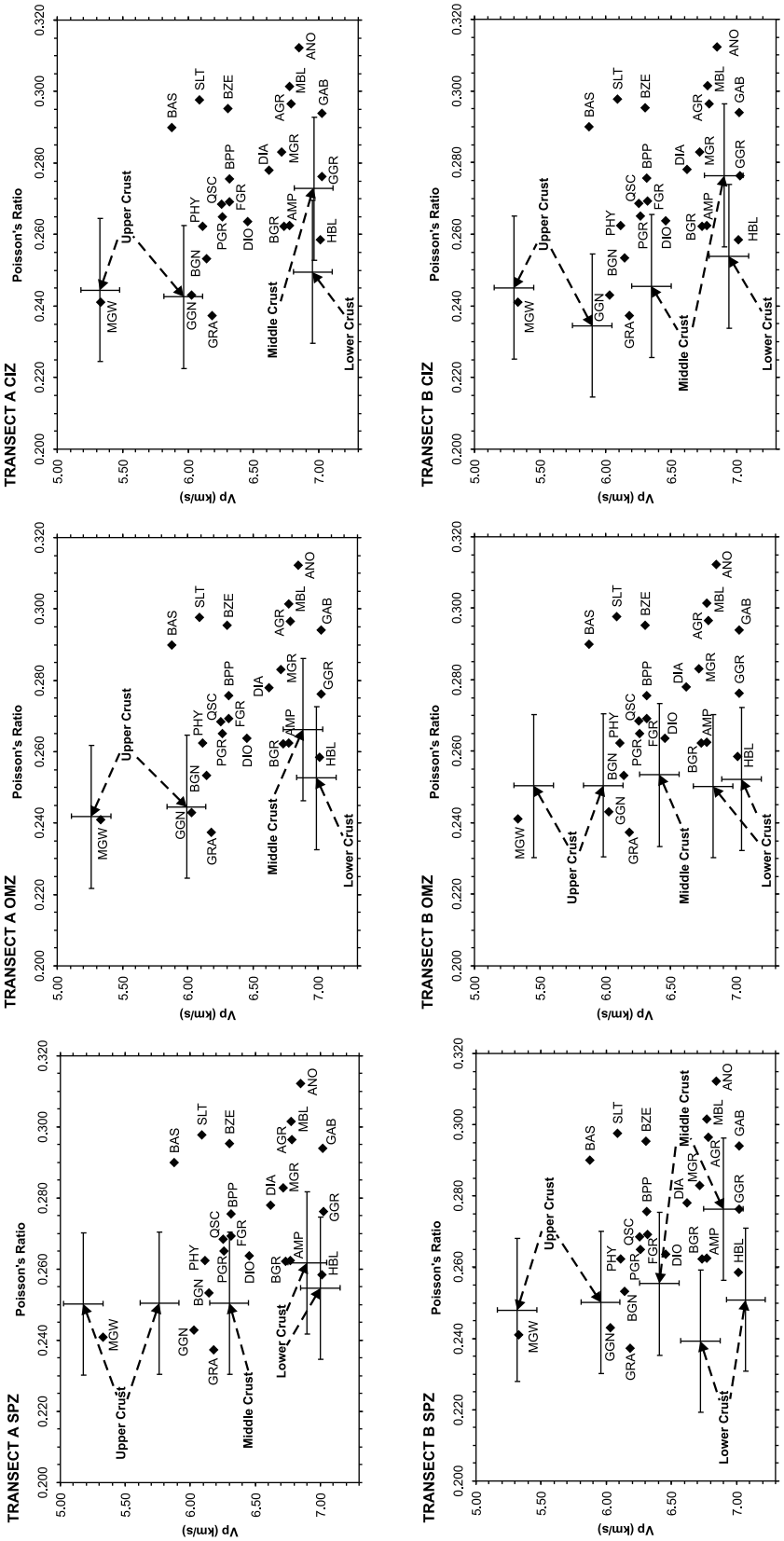

Figure 11. V_p versus Poisson's ratios for the rock types listed in Table 2 and the IBERSEIS-WA data. The vertical and horizontal lines represent the errors in the P wave velocities and Poisson's ratios determined from the IBERSEIS wide-angle data [*Palomeras et al.*, 2009] and this work, respectively.

basalt, diorite and metagabbro. The upper part of the middle crust within the CIZ shows similar V_p, around 6.4 km/s, but lower Poisson's ratio. The possible rock types for this area include: granite-granodiorite, paragranulite and diorite. The SPZ and CIZ present a lower-middle crust with high average P wave velocity and Poisson's ratio of 6.9 km/s and 0.28, respectively, values close to those found in transect A for the same area. The compatible rock types for this velocity and Poisson's ratio are: amphibolite, mafic granulite, mafic garnet granulite, anorthositic granulite, hornblendite, gabbro-norite-troctolite and greenschist facies basalt.

7.3. Lower Crust

[45] In transect A, within the SPZ, the lower crust is divided into two layers. The upper one has a P wave velocity of 6.9 km/s and a Poisson's ratio of 0.26. Consistent rock types with these values include: amphibolite, greenschist facies basalt, mafic granulite, hornblendite and mafic garnet granulite. Under this layer, the P wave velocity and Poisson's ratio are the same as in the OMZ and CIZ, namely 7.0 km/s and 0.25. Hornblendite is the rock type consistent with these values.

[46] For transect B, there are differences between the tectonic zones at lower crustal depths. Within the SPZ and OMZ there are two layers with different P wave velocity and Poisson's ratio. Under this layer, there are no differences between the tectonic zones. Within the SPZ there is a low-velocity layer underneath the middle crust, with P wave velocity of 6.7 km/s and Poisson's ratio of 0.24. The closest and most probable rock types for this depth in this region include: amphibolite and greenschist facies basalt. Within the OMZ there is also an upper lower crustal layer with P wave velocity equal to 6.8 km/s and Poisson's ratio equal to 0.25. Compatible rock types include: amphibolite, greenschist facies basalt and hornblendite. Underneath this layer, for all three tectonic zones, the P wave velocity and Poisson's ratio are 7.0 km/s and 0.25, respectively. Hornblendite is consistent with these values.

[47] In this correlation we have not considered the possibility of small-scale heterogeneity layers. It has to be taken into account that the values determined from the seismic data correspond to average values. Therefore, heterogeneous layers made up of a mixture of rock types consisting of mafic with less mafic material which would average the specific physical property values, should also be consistent with the seismic estimates. Thus, heterogeneous layered structures cannot be ruled out, and according to *Flecha et al.* [2009] should be considered.

8. Discussion

[48] The calculated Poisson's ratios for our two transects (Figures 5c and 6c) are quite similar. For the upper crust within the OMZ and CIZ, both transects show a low Poisson's ratio, being locally even less than 0.23 (Figures 5c and 6c). This is not the case for the middle crust, where high Poisson's ratios are obtained. At these depths, from 12 to 22 km, the Poisson's ratio is laterally variable with values that exceeds values of 0.28. In the lower crust different values are observed for each transect. On transect A the Poisson's ratio is constant along the whole transect with a value of 0.25. For transect B, at the same depth, the Poisson's ratio changes laterally, being higher within the CIZ (0.26) than within the SPZ (0.24). The difference between both transects is most probably due to the low resolution at these depths. Since no S wave intracrustal reflections have been identified in the shot gathers, no detailed information about the lower crust is achieved. For this reason, the lower crust has been modeled as a single layer in the V_s models. This is not the case in the V_p models, where it has been modeled in more detail, especially because the models include a low-velocity layer within the SPZ at ~23 km depth. This could explain the low Poisson's ratio at 20–25 km depth within the SPZ in transect B. This region has a lower V_p value than the others regions of the transect for the same depth but no difference has been detected for the V_s model. Accordingly, it results in a low Poisson's ratio.

[49] The uppermost crustal layer (first 2 km) presents differences between tectonic zones, but the only rock type compatible in all cases is metagraywacke. Since in this part of the crust the Poisson's ratio is strongly influenced by open crack porosity, we assume that the corresponding calculated Poisson's ratio is also influenced by this fact and does not strictly represent lithologies. Even then, these values are compatible with a rock type which agrees with the observed outcrops where the Paleozoic is represented by metagraywacke.

[50] The P wave models present high-velocity zones at midcrustal depths [*Palomeras et al.*, 2009], which are not as clear in the S wave velocity models. These high V_p areas correspond to the areas with high Poisson's ratio. According to *Christensen and Mooney* [1995] and *Christensen* [1996] the possible rock types that agree with the resulting high V_p

and high Poisson's ratio include: amphibolites, gabbro norite troctolite, mafic granulite, mafic garnet granulite, greenschist facies basalt and hornblendite. These velocities and Poisson's ratio also agree with measurements on gabbro samples collected in the area. The lower crust features little differences in P wave velocities and Poisson's ratio for both transects and all tectonic zones.

[51] The differences in the P wave velocities, the S wave velocities and the Poisson's ratio of the upper and middle crust between the tectonic provinces are also observed in multidisciplinary modeling studies [*Fernàndez et al.*, 2004; *Palomeras et al.*, 2011]. This supports the existence of different tectonic blocks, that accordingly could correspond to different terranes with variable characteristics and physical properties.

[52] The average V_p/V_s and, therefore, Poisson's ratio for the SW Iberia crust can be easily calculated. In most of the shot gathers, the *SmS* phase can be followed until 0 km where it intercepts the time axis at ~18 s twtt. The *PmP* phase intercepts the time axis at 0 km offset at ~10 s twtt [*Palomeras et al.*, 2009]. The depth of the Moho is fixed, therefore, $10V_p = 18V_s$. The resulting average V_p/V_s for the crust is 1.80 and the average Poisson's ratio is as high as 0.277. This indicates that the crust has a low SiO_2 content, i. e., it has a high content of mafic rocks. *Christensen and Mooney* [1995] constructed a 40 km deep crustal petrologic model based on a P wave velocity depth profile derived from a worldwide compilation of 560 seismic studies. The average V_p/V_s ratio estimated for this averaged continental crust is 1.768 and the Poisson's ratio is 0.265 [*Christensen*, 1996]. These values are lower than those obtained for the crust of SW Iberia.

[53] High Poisson's ratio at midcrustal levels together with the high P wave velocities at the same depths indicate that the mafic content in the middle crust is high, thus supporting the existence of intrusive mafic and ultramafic rocks of possible mantle origin. This agrees with the high-temperature/low-pressure metamorphism exhibited by midcrustal rocks and the origin of the mineralization found in the area [*Casquet et al.*, 2001; *Tornos et al.*, 2001; *Tornos and Casquet*, 2005] being explained by a thermal source (mantle-derived magma) interacting with middle crustal rocks. It also agrees with former interpretations derived from the IBERSEIS data set [*Simancas et al.*, 2003; *Carbonell et al.*, 2004; *Palomeras et al.*, 2009].

[54] At midcrustal levels, the normal incidence profile IBERSEIS images the IRB as a prominent high-amplitude reflective band [*Simancas et al.*, 2003; *Carbonell et al.*, 2004]. These authors suggest that, in order to account for the high reflectivity, the IRB must be made up of layers of rocks with variable seismic impedance, i.e., mafic, ultramafic and maybe some felsic rocks. These lenses can account for the high P wave velocities found at midcrustal levels and for the coda found in the seismic intracrustal phases [*Palomeras et al.*, 2009; *Flecha et al.*, 2009]. Accordingly, the velocities and Poisson's ratios calculated in this work do not need to be explained by a single lithology. The determined seismic velocities are more likely the average of a mixture of rocks.

9. Conclusions

[55] The close trace spacing wide-angle transects acquired in SW Iberia within the IBERSEIS experiment recorded high-amplitude S wave arrivals on the vertical component seismic recorders. Although only the first S wave arrivals (*Sg*), the Moho reflection (*SmS*) and the converted *PmS*/*SmP* phases can be correlated between shot gathers, the modeling strategy used allowed us to obtain two crustal V_s models, one along each transect. The resulting S wave velocity models show lateral differences between tectonic zones especially at upper and midcrustal depths thus supporting the existence of different tectonic terranes before the Variscan orogeny. At lower crustal levels smaller heterogeneities indicate the existence of syntectonic-posttectonic processes that have homogenized seismically the three zones. On average, the upper crust features a gradient from 2.90 km/s to 3.50 km/s within the SPZ, and from 3.10 km/s to 3.60 km/s within the OMZ and CIZ. The middle crust, from 12 to 20–22 km depth, features higher S waves velocities (+0.10 km/s) in the areas where the high P wave velocities are present. The lower crust features a S wave velocity gradient from 3.85 km/s at 20–22 km depth to 4.15 km/s at the Moho discontinuity. Poisson's ratio variations have been calculated from the resulting V_p and V_s models. The resulting Poisson's ratio for the crust also shows differences between tectonic zones. The upper crust features lower Poisson's ratio within the OMZ and CIZ than within the SPZ. At midcrustal depths, the areas with high P wave velocities and moderate S wave velocities feature high (more than 0.28) Poisson's ratio. These areas extend past the limit of the tectonic zones indicating postcollisional intraorogenic intrusion of mantle derived rocks. The lower crust features no lateral variations with a Poisson's ratio of

approximately 0.25. The average Poisson's ratio calculated for the whole crust in SW Iberia is higher than the one estimated for the average continental crust thus supporting the existence of a high content in mafic rocks. These velocity and Poison's ratio models indicate that although different terranes must have collided during the Variscan Orogeny, the proposed Early Carboniferous magmatic event must have affected the three tectonic zones. In the same way, a positive gravity anomaly characterizes SW Iberia, and mafic rocks are unusually frequent outcrop. All these evidences are interpreted as manifestations of the proposed Early Carboniferous magmatic event during the Variscan Orogeny. This event was synorogenic, affecting SW Iberia after the three collisional terranes shaping it (the SPZ, the OMZ and the CIZ) were already stuck.

Acknowledgments

[56] Funding for this research was provided by the Spanish Ministry of Education and Science through projects CGL200404623, CGL2007-63889, and TOPOIBERIA CONSOLIDER-INGENIO CSD2006-00041; the Generalitat de Catalunya (2005SGR00874); and the Junta de Andalucía. We thank the Associate Editor and anonymous reviewers for their constructive revisions and comments that improved the manuscript.

References

Araújo, A., P. Fonseca, J. Munhá, P. Moita, J. Pedro, and A. Ribeiro (2005), The Moura Phyllonitic Complex: Na Accretionary Complex related with the obduction in the southern Iberia Variscan Suture, *Geodin. Acta*, *18*, 375–383.

Ayarza, P., I. Palomeras, R. Carbonell, J. Afonso, and F. Simancas (2010), A wide-angle upper mantle reflector in SW Iberia: Some constraints on its nature, *Phys. Earth Planet. Inter.*, *181*(3–4), 88–102, doi:10.1016/j.pepi.2010.05.004.

Azor, A., F. González-Lodeiro, and J. Simancas (1994), Tectonic evolution of the boundary between the Central Iberian and Ossa-Morena zones (Variscan Belt, Southwest Spain), *Tectonics*, *13*, 45–61, doi:10.1029/93TC02724.

Azor, A., D. Rubatto, J. Simancas, F. González-Lodeiro, D. Martínez-Poyatos, L. Martín-Parra, and J. Matas (2008), Reic Ocean ophiolitic remnants in southern Iberia questioned by SHRIMP U-Pb zircon ages of Beja-Acebuches amphibolites, *Tectonics*, *27*, TC5006, doi:10.1029/2008TC002306.

Brown, D., R. Carbonell, I. Kukkonen, C. Ayala, and I. Golovanova (2003), Composition of the Uralide crust from seismic velocity (V-p, V-s), heat flow, gravity, and magnetic data, *Earth Planet. Sci. Lett.*, *210*(1–2), 333–349, doi:10.1016/S0012-821x(03)00143-2.

Burg, J., M. Iglesias, P. Laurent, P. Matte, and A. Ribeiro (1981), Variscan intracontinental deformation: The Coimbra-Córdoba Shear zone (SW Iberian Peninsula), *Tectonophysics*, *78*, 161–177, doi:10.1016/0040-1951(81)90012-3.

Carbonell, R., F. Simancas, C. Juhlin, J. Pous, A. Pérez-Estaún, F. González-Lodeiro, G. Muñoz, W. Heise, and P. Ayarza (2004), Geophysical evidence of a mantle derived intrusion in SW Iberia, *Geophys. Res. Lett.*, *31*, L11601, doi:10.1029/2004GL019684.

Carmichael, R. S. (1989), *Physical Properties of Rocks and Minerals*, CRC Press, Boca Raton, Fla.

Casquet, C., C. Galindo, F. Tornos, F. Velasco, and A. Canales (2001), The Aguablanca Cu-Ni ore deposit (Extremadura, Spain), a case of synorogenic orthomagmatic mineralization: Age and isotope composition of magmas (Sr, Nd) and ore (S), *Ore Geol. Rev.*, *18*, 237–242, doi:10.1016/S0169-1368(01)00033-6.

Castro, A., C. Fernández, J. de la Rosa, I. Moreno-Ventas, and G. Rogers (1996), Significance of MORB-derived amphibolites from the Aracena metamorphic belt, southwest Spain, *J. Petrol.*, *37*, 235–260.

Christensen, N. (1996), Poisson's ratio and crustal seismology, *J. Geophys. Res.*, *101*(2), 3139–3156.

Christensen, N., and W. Mooney (1995), Seismic velocity structure and composition of the continental crust: A global view, *J. Geophys. Res.*, *100*(B6), 9761–9788, doi:10.1029/95JB00259.

Eden, P., and J. Andrews (1990), Middle to Upper Devonian mélanges in SW Spain and their relationship to the Meneage Formation in South Cornwall, *Proc. Ussher Soc.*, *7*, 217–222.

Fernàndez, M., I. Marzán, and M. Torne (2004), Lithospheric transition from the Variscan Iberian Massif to the Jurassic oceanic crust of the central Atlantic, *Tectonophysics*, *386*(1–2), 97–115, doi:10.1016/j.tecto.2004.05.005.

Flecha, I., I. Palomeras, R. Carbonell, F. Simancas, P. Ayarza, J. Matas, F. González-Lodeiro, and A. Peréz-Estaún (2009), Seismic imaging and modelling of the lithosphere of SW-Iberia, *Tectonophysics*, *472*(1–4), 148–157,doi:10.1016/j.tecto.2008.05.033.

Fonseca, P., and A. Ribeiro (1993), Tectonics of the Beja-Acebuches Ophiolite: A major suture in the Iberian Variscan Foldbelt, *Geol. Rundsch.*, *82*, 440–447.

Fonseca, P., J. Munhá, F. Rosas, P. Moita, A. Araujo, and N. Leal (1999), Variscan ophiolites and high-pressure metamorphism in southern Iberia, *Ofioliti*, *24*, 259–268.

Gómez-Pugnaire, M., A. Azor, J. Fernández-Soler, and V. L. Sánchez-Vizcaíno (2003), The amphibolites from the Ossa-Morena/Central Iberian Variscan suture (Southwestern Iberian Massif): Geochemistry and tectonic interpretation, *Lithos*, *68*, 23–42, doi:10.1016/S0024-4937(03)00018-5.

Hauser, F., B. M. O'Reilly, P. W. Readman, J. S. Daly, and R. van den Berg (2008), Constraints on crustal structure and composition within a continental suture zone in the Irish Caledonides from shear wave wide-angle reflection data and lower crustal xenoliths, *Geophys. J. Int.*, *175*(3), 1254–1272, doi:10.1111/j.1365-246X.2008.03945.x.

Hawman, R. B., R. H. Colburn, D. A. Walker, and S. B. Smithson (1990), Processing and inversion of refraction and wide-angle reflection data from Nevada Passcal Experiment, *J. Geophys. Res.*, *95*(B4), 4657–4691.

Holbrook, W. (1988), An interpretation of wide-angle compressional and shear wave data in southwest Germany: Poisson's ratio and petrological implications, *J. Geophys. Res.*, *93*(B10), 12,081–12,106.

Jacob, A. W. B., and D. C. Booth (1977), Observation of PS reflections from the Moho, *J. Geophys.*, *43*, 687–692.

Janik, T., E. Kozlovskaya, P. Heikkinen, J. Yliniemi, and H. Silvennoinen (2009), Evidence for preservation of crustal root beneath the Proterozoic Laplan-Kola orogen (northern Fennoscandian shield) derived from P and S wave velocity models of POLAR and HUKKA wide-angle reflection and refraction profiles and FIRE4 reflection transect, *J. Geophys. Res.*, *114*, B06308, doi:10.1029/2008JB005689.

Matte, P. (2001), The Variscan collage and orogeny (480–290 Ma) and the tectonic definition of the Armonica microplate: A review, *Terra Nova*, *13*, 122–128.

Oliveira, J. (1990), Stratigraphy and synsedimentary tectonism, in *Pre-Mesozoic Geology of Iberia*, part VI, *South Portuguese Zone*, pp. 348–362, Springer, Berlin.

Ordoñez Casado, B. (1998), Geochronological studies of the pre-Mesozoic basement of the Iberian Massif: The Ossa-Morena zone and the allochthonous complexes within the Central Iberian zone, Ph.D. thesis, ETH Zurich, Zurich, Switzerland.

Palomeras, I., et al. (2009), The nature of the lithosphere across the Variscan Orogen of SW-Iberia: Dense wide-angle seismic reflection data, *J. Geophys. Res.*, *114*, B02302, doi:10.1029/2007JB005050.

Palomeras, I., R. Carbonell, P. Ayarza, M. Fernández, F. J. Simancas, D. Martínez Poyatos, F. González-Lodeiro, and A. Pérez-Estaún (2011), Geophysical model of the lithosphere across the Variscan Belt of SW-Iberia: Multidisciplinary assessment, *Tectonophysics*, doi:10.1016/j.tecto.2010.07.010, in press.

Pérez-Estaún, A., and F. Bea (2004), Macizo Ibérico, in *Geología de España*, pp. 21–230, Soc. Geol. de España, Madrid.

Pin, C., and J. Rodríguez (2009), Comment on "Rheic Ocean ophiolitic remnants in southern Iberia questioned by SHRIMP U-Pb zircon ages on the Beja-Acebuches amphiolites" by A. Azor et al., *Tectonics*, *28*, TC5013, doi:10.1029/2009TC002495.

Pous, J., G. Muñoz, W. Heise, J. Melgarejo, and C. Quesada (2004), Electromagnetic imaging of Variscan crustal structures in SW Iberia: The role of interconnected graphite, *Earth Planet. Sci. Lett.*, *217*(3–4), 435–450, doi:10.1016/S0012-821X(03)00612-5.

Quesada, C., P. Fonseca, J. Munhá, J. Oliveira, and A. Ribeiro (1994), The Beja-Acebuches Ophiolite (Southern Iberia Variscan fold belt): Geological characterization and geodynamic significance, *Bol. Geol. Minero*, *105*, 3–49.

Robardet, M., and J. Gutíerrez-Marco (2004), The Ordovician, Silurian and Devonian sedimentary rocks of the Ossa-Morena Zone (SW Iberian Peninsula, Spain), *J. Iberian Geol.*, *30*, 73–92.

Sáez, R., E. Pascual, M. Toscano, and G. R. Almodóvar (1999), The Iberian type of volcano-sedimentary massive sulphide deposits, *Mineral. Deposita*, *34*, 549–570.

Schmelzbach, C., J. Simancas, C. Juhlin, and R. Carbonell (2008), Seismic-reflection imaging over the South Portuguese Zone Fold-and-Thrust belt, SW Iberia, *J. Geophys. Res.*, *113*, B08301, doi:10.1029/2007JB005341.

Shillington, D. J., H. Van Avendonk, W. D. Holbrook, P. B. Kelemen, and M. J. Hornbach (2004), Composition and structure of the central Aleutian island arc from arc-parallel wide-angle seismic data, *Geochem. Geophys. Geosyst.*, *5*, Q10006, doi:10.1029/2004GC000715.

Simancas, F., D. M. Poyatos, I. Expósito, A. Azor, and F. González-Lodeiro (2001), The structure of a major suture zone in the SW Iberian Massif: The Ossa-Morena/Central Iberian contact, *Tectonophysics*, *332*(1–2), 295–308, doi:10.1016/S0040-1951(00)00262-6.

Simancas, F., et al. (2003), Crustal structure of the transpressional Variscan orogen of SW Iberia: SW Iberia deep seismic reflection profile (IBERSEIS), *Tectonics*, *22*(6), 1062, doi:10.1029/2002TC001479.

Simancas, J. F., et al. (2006), Transpresional collision tectonics and mantle plume dynamics: The Variscides of southwestern Iberia, in *European Lithosphere Dynamics*, vol. 32, pp. 345–354, Geol. Soc., London.

Simancas, J., A. Azor, D. M. Poyatos, A. Tahiri, H. E. Hadi, F. González-Lodeiro, A. Pérez-Estaún, and R. Carbonell (2009), Tectonic relationships of southwest Iberia with the allochthons of northwest Iberia and the Moroccan Variscides, *C. R. Geosci.*, *341*, 103–113, doi:10.1016/j.crte.2008.11.003.

Tornos, F., and C. Casquet (2005), A new scenario for related IOCG and Ni-(Cu) mineralization: The relationship with giant mid-crustal mafic sills, Variscan Iberian Massif, *Terra Nova*, *17*(3), 236–241, doi:10.1111/j.1365-3121.2005.00601.x.

Tornos, F., C. Casquet, C. Galindo, F. Velasco, and A. Canales (2001), A new style of Ni-Cu mineralization related to magmatic breccia pipes in a transpressional magmatic arc, Aguablanca, *Mineral. Deposita*, *36*, 700–706, doi:10.1007/s001260100204.

Wang, Q., and J. Shaocheng (2009), Poisson's ratios of crystalline rocks as a function of hydrostatic confining pressure, *J. Geophys. Res.*, *114*, B09202, doi:10.1029/2008JB006167.

Zelt, C., and R. Smith (1992), Seismic traveltime inversion for 2-D crustal velocity structure, *Geophys. J. Int.*, *108*(1), 16–34.

Zeyen, H., and M. Fernàndez (1994), Integrated lithospheric modeling combining thermal, gravity, and local isostacy analysis: Application to the NE Spanish Geotransect, *J. Geophys. Res.*, *99*, 18,089–18,102.